MONOCULAR PASSIVE RANGING BY AN OPTICAL SYSTEM WITH BAND PASS FILTERING

THESIS

Joel R. Anderson, Captain, USAF

AFIT/GAP/ENP/10-M01

DEPARTMENT OF THE AIR FORCE
AIR UNIVERSITY

AIR FORCE INSTITUTE OF TECHNOLOGY

Wright-Patterson Air Force Base, Ohio

AFIT/GAP/ENP/10-M01

MONOCULAR PASSIVE RANGING BY AN OPTICAL SYSTEM WITH BAND PASS FILTERING

THESIS

Presented to the Faculty

Department of Engineering Physics

Graduate School of Engineering and Management

Air Force Institute of Technology

Air University

Air Education and Training Command

In Partial Fulfillment of the Requirements for the

Degree of Master of Science in Applied Physics

Joel R. Anderson, BS, MS

Captain, USAF

March 2010

AFIT/GAP/ENP/10-M01

MONOCULAR PASSIVE RANGING BY AN OPTICAL SYSTEM WITH BAND PASS FILTERING

Joel R. Anderson, BS, MS

Captain, USAF

Approved:

//SIGNED//	
Glen P. Perram, PhD (Chairman)	Date
//SIGNED//	
Kevin C. Gross, PhD (Member)	Date
//SIGNED//	
Lt Col Michael R. Hawks (Member)	Date

Abstract

An instrument for monocular passive ranging based on atmospheric oxygen absorption near 762 nm has been designed, built and deployed to track emissive targets, including the plumes from jet engines or rockets. An intensified CCD array is coupled to variable band pass liquid crystal display filter and 3.5 – 8.8 degree field of view optics to observe the target. By recording sequential images at 7 Hz in three 6 nm width bands, the transmittance of the R-branch of the O_2 (X-b) (0,0) band is determined. A metric curve for determining range from transmittance is developed using the HITRAN spectral database. A low cost system was designed and ground tested at ranges of 50 -380 m using halogen and incandescent light sources, establishing an average range error of 12%. The system was first deployed for a ground test viewing an F-16 in afterburner at ranges of 0.35 – 4.8 km, establishing a range error of 15% despite the presence of optical turbulence and a structured source spectrum. Finally, the instrument was flight tested in a C-12 imaging an F-16 in afterburner at ranges up to 11 km. The target was manually tracked, and pointing jitter limited image interpretation. A study of range error as a function of signal-to-noise ratio produced superior results to previous methods using Fourier Transform Spectroscopy. However, increased signal relative to background scatter will be required for accurate ranging for these tactical air-to-air scenarios. The promise for improved instrument performance is discussed.

Acknowledgments

I would like to express my sincere appreciation to my research advisors, Dr. Glen Perram and Dr. Kevin Gross, for the ideas, guidance and support they offered me during this research. I would, also, like to thank the Air Force Test Pilot School for sponsoring this project and thank everyone there that helped to install this system onto the C-12 for the flight test. I would especially like to thank the entire Air Cyclops test management project team (Cain'n, SERJ, Scrabble, and Noζ) for their work and efforts.

Most of all, I would like to thank and express my sincere appreciation to my wife and children. Their assistance in the final testing was crucial. They suffered through my work, and helped me to enjoy life while not working, to give me the energy to work when I had to.

Joel R. Anderson

Table of Contents

List of Figures

Figure Page

List of Tables

Table Page

List of Symbols, Abbreviations, and Acronyms

AFB	Air Force Base
AFIT	Air Force Institute of Technology
AMPR	Advanced Monocular Passive Ranging
α	absorption coefficient
ATM	atmosphere
C	Celcius
HITRAN	High-Resolution Transmission Molecular Absorption
ICCD	Intensified Charge Coupled Device
K	Kelvin
km	kilometer
λ	wavelength
LCD	Liquid Crystal Display
m	meter
mBar	Millibar
MPR	Monocular Passive Ranging
nm	nanometer
OPRS	Oxygen Passive Ranging System
SNR	Signal to Noise Ratio
TPS	Test Pilot School
USAF	United States Air Force

MONOCULAR PASSIVE RANGING BY AN

OPTICAL SYSTEM WITH BAND PASS FILTERING

I. Introduction

The contents of this thesis describe the research and development of a passive ranging system that was designed to estimate range to an emissive target such as a jet exhaust or rocket plume. This research was accomplished as part of a combined program between the Air Force Institute of Technology (AFIT) and the USAF Test Pilot School (TPS). The system was designed and built at AFIT. Initial experimentation and testing of the system was accomplished at AFIT. The system was further developed at TPS and installed on a C-12C aircraft. It was then ground and flight tested by the Air Cyclops test management project team as part of the school curriculum.

Background

The most proliferated methods to accurately estimate range to a target utilize an active system such as radar. This means they actively radiate electromagnetic waves that strike the target and are reflected back to the sensor. By precisely measuring the time for the electromagnetic waves to propagate to the target and return to the sensor, an accurate range can be determined. These active ranging systems are effective against many different target types in many different conditions. Passive ranging systems do not

radiate any electromagnetic energy, but instead rely on electromagnetic waves that are either emitted from the target or are reflected off the target from other sources such as a light or the sun. Passive ranging is not as versatile and generally not as accurate as active ranging, but due to their stealth characteristics these systems are still highly desired for some applications. As a result, many different passive ranging systems exist for different conditions, and they operate using several different principles.

Two systems that estimate range based on reflected light are described below. One principle is stereo ranging. This is the same principle that gives people depth perception. By simply observing something using both eyes, the brain can estimate how far away objects are. Fielded systems like this use two or more sensors that are in known locations observing the same target. By knowing the sensor locations and applying geometry, the target location or range can be estimated. One drawback of this system is that the sensors must communicate with each other to verify the same target is selected. High accuracy at long ranges also requires the sensors to be located far apart. People also use a second type of passive ranging when only using one eye. This is one type of monocular passive ranging. When using only one eye, the brain recognizes an object such as a doorway, and knows what size that doorway should be. The brain then compares how big the doorway looks and how big it thinks the doorway is. If the doorway is large, it estimates that it is close. If it is small, the brain assumes the doorway is far away. Systems that use this type of passive ranging must recognize a target and then know the true size of the target to estimate the range. The major drawback to this type of system is that if the object cannot be identified, no range estimate can be made.

Also, if the target is misidentified, or is a different size that what is expected, the range information will be incorrect.

The second type of passive ranging exploits emitted light to estimate target range. This is where the current research is focused, and it is designed to estimate range to a target such as a headlight, a jet plume, or a rocket plume. This type of monocular passive ranging utilizes the precisely modeled absorption characteristics of the atmosphere to estimate how much of the signal was absorbed while propagating through the atmosphere, and then compares that to measured spectra to estimate the target range. While this method also has drawbacks, it is advantageous in that no prior target information is required for estimating range, and it accomplishes this ranging with a single detector. This type of monocular passive ranging has been attempted for the past 15 years with varying success, but the process continues to be refined and improved. This research intends to aid the improvement of future systems.

Motivation

The Department of Defense has always been interested in devices that determine range to a target. Many technologies exist today that accurately determine this range in an active manner using traditional radar and laser radar devices. Although the range information is very accurate, there is a drawback to these systems. In addition to providing range information, they also transmit an electromagnetic signature which can be exploited to alert the target that someone or something is out there observing them. It can even be used to provide information about the radar source and information about the source location.

The current military battle space requires an ability to obtain range information in a covert manner. Several uses for this type of system exist. One of these possible uses is as part of an aircraft defensive system. When an aircraft is under missile attack either from the ground or the air, the aircraft has limited options to evade the missile. The application of chaff, flares, and other defensive maneuvers need to be applied at specific times and aspect angles to have the greatest probability of success. In this case, it would be highly desirable for the crew of the aircraft under attack to know the range and bearing of the incoming missile. Using an active ranging system in this case could act as a homing signal with catastrophic results. In this situation, a passive ranging system would be highly advantageous.

Another great application for this technology would be for the YAL-1A Airborne Laser weapon system. This is a modified Boeing 747-400F with a megawatt class chemical oxygen iodine laser. This system was designed to loiter near hostile territory, then track and shoot down theater ballistic missiles in the boost phase. In this scenario, the airspace surrounding the aircraft must be continually searched for missiles and when one or more missiles are airborne, each missile must be located and prioritized according to its range and trajectory. A monocular passive ranging system as part of this weapons system could enhance its ability to locate and prioritize multiple targets with a smaller signature and using less energy than a radar system. This information could then be sent to an active laser system for close tracking and missile shoot-down.

Problem Statement

Can a monocular passive ranging system that utilizes band pass filters to estimate the atmospheric absorption accurately estimate range to an emissive target?

Research Approach

An effective and accurate monocular passive ranging system was developed that used a spectrometer as the sensor and atmospheric oxygen at 762 nanometers (nm) as the absorbing species (Hawks, 2006). The purpose for this current research was an attempt to simplify the design to demonstrate that the system could be easily miniaturized and used in a militarily significant application without a complex construct. There were several constraints that all led to the design that was chosen. First, the final system needed to be installed on an aircraft and image a moving target from an airborne vantage point. Also, the funding was limited and required the system design to consist primarily of existing AFIT owned equipment. Budget constraints, combined with the required imaging sensitivity, drove the design to utilize a single sensor. An automatic tracking system was too expensive, which yielded a design with a wide field of view that required manual target tracking. Imaging moving targets and correlating the filter band pass images to times and target ranges was accomplished through the purchase of a digitally tunable band pass filter. The final system used a single imaging detector and three cycling band pass filters to provide the necessary spectral information for estimating the oxygen absorption. This system was developed and then taken to the USAF TPS where it was installed in a C-12 aircraft and tested airborne using an F-16 afterburning plume as a target. A large portion of the work accomplished for this thesis was designing and

building the system as well as programming the software which was required for proper data acquisition and post-flight image analysis.

Document Structure

Chapter 2 is a review of some of the previous monocular passive ranging systems that have been attempted. It will also review atmospheric transmission and give some background on the HITRAN database. Chapter 3 contains the body of a scholarly article which documents this research. This article had not been published at the time this thesis was completed, but was intended for submission to SPIE. Chapter 4 contains additional results from the initial testing as well as follow-on testing which were not discussed in Chapter 3. Chapter 5 summarizes the research, final conclusions, and significance of this research. This also suggests possible future research areas that could enhance this system. Three appendices provide more information about the passive ranging system. Appendix A includes the methods used for various aspects of the system calibration. Appendix B includes tables of atmospheric conditions for the tests that were accomplished. Appendix C includes some of the software code that was written to enable the data acquisition and analysis.

II. Literature Review

This literature review includes discussions on a few of the previously attempted monocular passive ranging systems that are similar to the current research. The basic concept of these systems is based on the properties of atmospheric transmission and molecular absorption. Therefore, this chapter also includes a discussion on this topic. The literature review is concluded with a description of the atmospheric model used in this research.

Monocular Passive Ranging

In the mid 1990's, a theory was developed (Jeffrey and others, 1994) that used Beer's Law to estimate the range to an emissive target. This was popularly known as monocular passive ranging (MPR). This method used the ratios of the atmospheric attenuation of two different carbon dioxide absorption bands in the mid wave infrared to solve Beer's Law for the path length. This approach made several simplifying assumptions that did not prove robust. First, Beer's Law applies only to monochromatic light. Since the measurement bands were finite, the strict application of Beer's Law was flawed. This introduced errors that were not easy to overcome. The MPR theory also assumed that the ratio of source intensities between absorption bands would be known (Evans and Hibbeln, 1996). Although this ratio could be estimated, it was an unknown and introduced more error to the system than was originally estimated. This method also used models to calculate the difference in scattering losses between the bands, which required careful characterization of the atmosphere and was more difficult to estimate

than was originally believed. The basic idea of MPR was good, but more work was required to reduce these errors.

Advanced Monocular Passive Ranging

Another program sought to improve on this theory, and is called advanced monocular passive ranging (AMPR). This method was developed by Opto-Knowledge Systems Inc., and used an imaging spectrometer (Scriven, 2008). This method built on the MPR theory by comparing multiple spectral absorption bands for the calculations instead of just a ratio of two. Also, instead of calculating the range strictly from Beer's Law, the AMPR system operated by estimating both atmospheric conditions and range and comparing the resulting theoretical spectrum to the observed spectrum. The theoretical spectrum was then iterated using different input parameters, including range. The range was determined as the range for which the theoretical spectrum matched the observed spectrum the closest. Atmospheric conditions at the sensor and atmospheric models provided the system with initial conditions to begin the iterations. This system was implemented to provide range estimates real-time, and had varied success. Initial testing showed range errors greater than 35%, but following some refinements to the algorithm, range errors were reduced to below 10%. This method still, however, required large and complex equipment.

Atmospheric Oxygen Passive Ranging

One additional approach to passive ranging (Hawks, 2006) used the absorption of atmospheric oxygen to estimate target range. Photons with wavelengths near 762 nm excite an electronic transition of oxygen and are absorbed as they pass through the

atmosphere. This method measured the transmitted target signal with a Fourier transform spectrometer and compared the depth of the absorption feature to the level of the baseline spectrum to determine a total absorption factor. This method used the principle of Beer's Law, but accounted for its monochromatic limitation by using band models to describe the broadband absorption. The measured spectrum was used to determine the amount of oxygen absorption which occurred upon atmospheric propagation. This value was then compared to model predictions for the expected absorption versus range given the current atmospheric conditions of temperature, pressure and humidity to find a range estimate. One advantage of this method is that transmission losses not associated with the absorption, such as scattering and turbulence (which caused difficulties for MPR) do not need to be known since they effect not just the absorption feature, but also the out of band baseline measurements. By comparing the depth of the absorption feature to the baseline, these other effects are naturally accounted for.

This method was the basis for the current research and will be described more fully in the following chapter. This system still used expensive and sensitive equipment, so the current research looked to implement this method for use with an imaging camera that used three band pass filters to estimate the atmospheric oxygen absorption instead of a spectrometer.

Atmospheric Transmission

As light propagates through the atmosphere, the signal is attenuated so that the intensity is higher at the source than at the destination. Transmission is defined as the fraction of the source intensity that actually arrives at the destination. There are three

main principles that effect the signal transmission along its course. The first is absorption, which means that some of the energy transmitted from a source is transferred from the light to the molecules that make up the atmosphere through which it propagates. The second effect is the scattering of the light. This means that light does not take a direct path as it passes through the atmosphere, but it instead strikes molecules which change its direction. A third atmospheric effect is turbulence. Turbulence also causes a change to the transmission of the light, but instead of changing its overall direction or intensity, it just causes fluctuations in the signal resulting in image blurring. These three effects are described in more detail below.

Molecular Absorption

Each molecule along the line of sight; such as oxygen, nitrogen, or water vapor; can participate in absorption, and the net attenuation of the input signal is described by Beer's Law:

$$I = I_o \, e^{(-\alpha(\lambda)L)} \tag{1}$$

where

I = *observed intensity* (W/m^2)

I_o = *source intensity* (W/m^2)

α = *absorption coefficient* (m^{-1})

λ = *wavelength* (m)

L = *path length* (m)

The amount of absorption is a function of the path length through the atmosphere and the wavelength dependent absorption coefficient. Absorption attenuates the signal as it passes through the atmosphere, and is in most cases undesirable. In the case of MPR, however, this absorption is utilized to estimate the path length (or range). Figure 1 shows a sample transmission spectrum from a solid rocket motor which was obtained during a passive ranging test at Edwards AFB, CA (Hawks, 2006). For this thesis, the oxygen absorption feature at 762 nm will be used. Note that the depth of this feature is proportional to the path length to the source. Also seen in Figure 1 are two strong potassium spikes at slightly higher wavelengths (767 nm and 770 nm). These are typical of rocket type plumes, and need to be accounted for in an accurate ranging system.

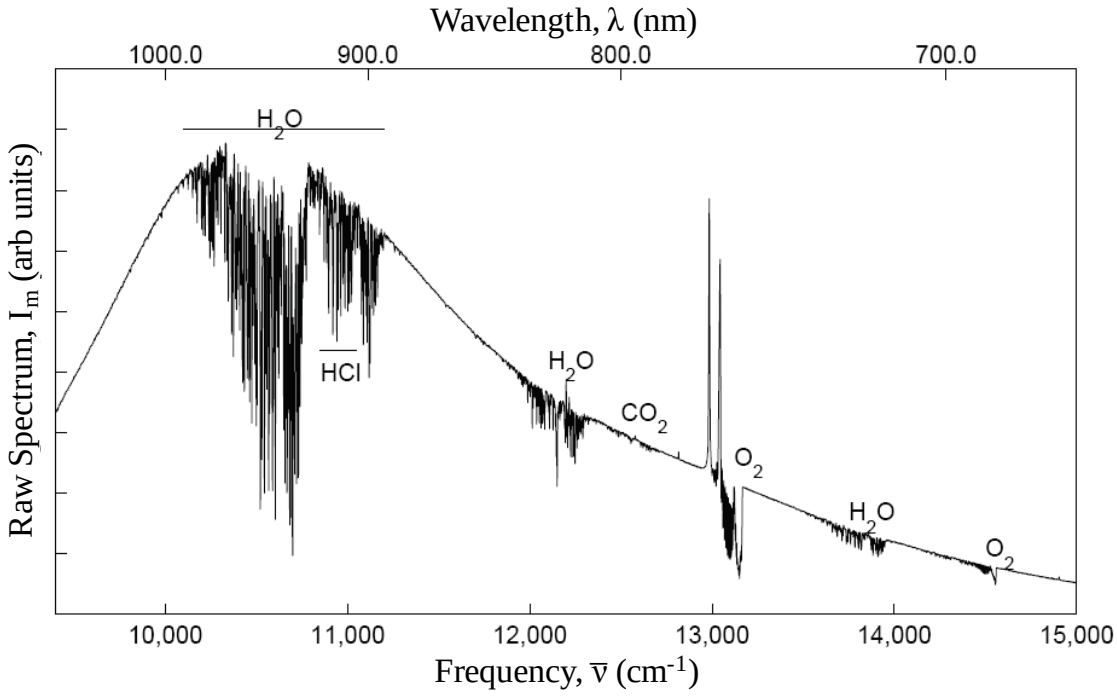

Figure 1. Sample Solid Rocket Motor Spectrum (Hawks, 2006)

Scattering

Besides the atmospheric molecules absorbing photons from the beam, they also scatter photons. Scattering losses also obey Beer's Law. The scattering coefficient varies according to the size of the molecules. For particles that are much smaller than the photon wavelength, Rayleigh (or molecular) scattering occurs. In this case, the scattering coefficient α_R is proportional to λ^{-4} (Andrews and Phillips, 2005). The blue appearance of the sky is a result of Rayleigh scattering. Since the wavelength of blue light is shorter than the red, yellow, and green wavelengths, the blue is scattered more strongly and seen by our eyes. A second type of scattering is called Mie (or aerosol) scattering. This occurs when the transmitted light interacts with particles that are near the same length or larger than the photon wavelength. Aerosols such as smoke, dust, and water droplets cause this interference. The difficulty in seeing through haze and fog is a result of Mie scattering. The light scatters off of these aerosols and the light does not make it to our eyes. Geographic location is very important in Mie scattering, and since the average aerosol sizes can vary between 0.03μm to 8μm (Sprangle and others, 2007), passive ranging systems which required accurate estimates of scattering have had difficulties. Scattering also poses a problem for the current research. Instead of the scattering of the light away from the sensor being the issue, the scattering processes also causes non-target radiation to scatter into the sensor which affects the results.

Turbulence

Turbulence can also cause a spreading of the propagated light. Turbulence occurs when temperature gradients in the atmosphere cause a variation in the index of refraction of the air. This index of refraction change causes random beam movements or

scintillation. The effect of turbulence is what causes the blurring when observing a hot asphalt road. Turbulence is only weakly proportional to the inverse of the wavelength ($\lambda^{-1/5}$) (Andrews and Phillips, 2005) and does not cause an average reduction in the transmission, but causes it to vary with time.

High-Resolution Transmission Molecular Absorption Database

To estimate range using the monocular passive ranging theory, an accurate model of the atmosphere must be used. For this research, the high-resolution transmission molecular absorption (HITRAN) database was used. The HITRAN database was created in the late 1960's by the Air Force Cambridge Institute Laboratories to help the Air Force characterize the infrared properties of the atmosphere (Rothman and others, 2009). The original database included seven major molecular species in the atmosphere in the infrared regime. This validated database is now the recognized international standard and contains 42 molecular species and is maintained by the Harvard-Smithsonian Center for Astrophysics in Cambridge, Massachusetts. This database was accessed by a line by line radiative transfer model that took input parameters of temperature, pressure, relative humidity, and path length and output the optical cross section of the atmosphere. This result was then sampled at every 0.002 nm.

III. Oxygen Based Passive Ranging Using Band Pass Filters

The following chapter is the body of a scholarly article which discusses the theory, design, and testing of the oxygen passive ranging system (OPRS). The abstract and the introduction have been removed to eliminate redundancy in this thesis.

Oxygen Passive Ranging System

Theory

As light propagates through the atmosphere, each molecule such as oxygen, nitrogen, or water vapor will absorb photons from the light according to Beer's Law (Equation 1). Transmission ($\mathcal{T}$) and absorption (A) describe how much the light is effected and are defined as

$$\mathcal{T} = \frac{I}{I_o} \tag{2}$$

$$A = 1 - \mathcal{T} \tag{3}$$

The amount of absorption is a function of the path length through the atmosphere and the wavelength dependent absorption coefficient. This absorption is in most cases undesirable, yet here is utilized to estimate the path length (or range). The current work uses the oxygen absorption feature at 762 nm as seen in Figure 1. Also note the two strong potassium peaks which are typical of rocket fuel impurities. There was no potassium expected in the targets used in this research, so the OPRS, as currently configured is not expected to perform well against targets that contain potassium.

To estimate target range based on the depth of the oxygen absorption feature, first the depth of this feature, or transmission in this region, must be measured. This measurement must then be compared to model predictions of how the transmission in this region varies with range, temperature, pressure, and humidity.

To measure the transmission due to atmospheric oxygen in this region, three band pass filters which were centered on 778 nm, 762 nm, and 752 nm were used with a camera. A depiction of these band pass filters overlaid onto a model prediction of the oxygen absorption feature is shown in Figure 2.

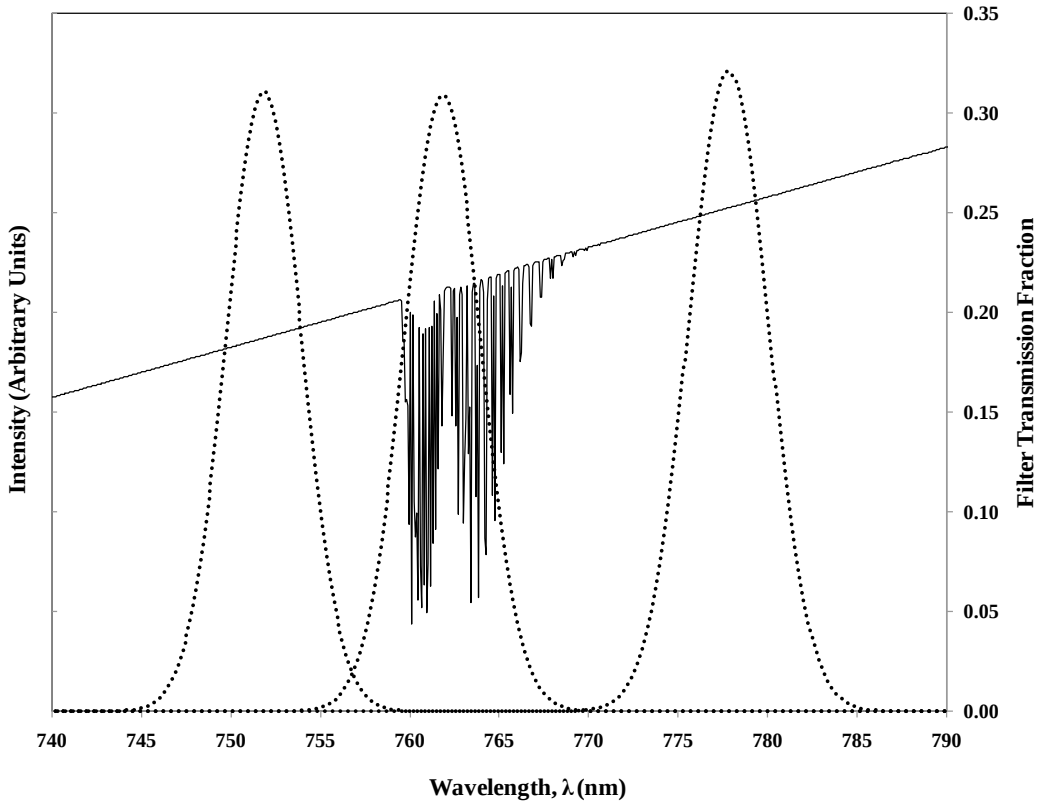

Figure 2. HITRAN Prediction of Oxygen Absorption Overlaid with the OPRS Band Filters

The intensities of each of the three band pass filtered measurements as recorded on the camera can be described by the following equation:

$$I = I_o \cdot \mathcal{T}_{Turb} \cdot \mathcal{T}_{Scatt} \cdot \mathcal{T}_{O2} \cdot \mathcal{T}_{Filter} \cdot R_{Cam} \quad (4)$$

where

I = *observed intensity* (W/m^2)

I_O = *source intensity* (W/m^2)

$\mathcal{T}_{Turb}$ = *transmission due to turbulence* (fraction)

$\mathcal{T}_{Scatt}$ = *transmission due to scattering* (fraction)

$\mathcal{T}_{O2}$ = *transmission due to atmospheric Oxygen* (fraction)

$\mathcal{T}_{Filter}$ = *transmission due to band pass filter* (fraction)

R_{Cam} = *camera spectral response* (fraction)

For each of the three filter band passes, the intensities, transmission factors, and the detector spectral responses will be different. To begin solving this equation, the source intensity, the transmission losses due to scattering, and the transmission losses due to turbulence will be combined together to create a baseline signal intensity. Equation 4 can now be rewritten to define this baseline signal intensity (I'_o):

$$I'_o = I_o \cdot \mathcal{T}_{Turb} \cdot \mathcal{T}_{Scatt} = \frac{I}{\mathcal{T}_{O2} \cdot \mathcal{T}_{Filter} \cdot R_{Cam}} \quad (5)$$

The oxygen transmission is initially assumed to be 1 for the outer bands (778 nm band pass and the 752 nm band pass). The filter transmission and the camera spectral response can be measured; therefore, the baseline intensities for the outer bands can be solved directly. Since the turbulence and scattering are largely broadband effects

(Hasson and Dupuis, 2002) they are assumed to be linear over this region from 740 nm to 790 nm. To estimate the baseline intensity for the 762 nm band pass measurement, the source intensity will also be assumed linear over this same region. This enables calculation of the baseline signal intensity for the 762 nm band by using a simple linear interpolation of the outer band baseline intensities. The oxygen transmission assumption should be good, but for the Gaussian shaped filters used, there was some overlap of the tails with the absorption feature which resulted in reduced transmission at long ranges. This was accounted for in the end by iterating this process accounting for oxygen transmission less than 1. Equation 5 is then re-written to solve for the measured transmission:

$$\mathcal{T}_{O2}^{'} = \frac{I}{I_o' \cdot \mathcal{T}_{Filter} \cdot R_{Cam}} \tag{6}$$

This measured transmission must then be compared to model predictions of transmission versus range to estimate the target range.

To obtain this relationship between theoretical transmission and range, refer to Beer's Law in its exact form:

$$\mathcal{T}_{O2}(\lambda, L) = \exp\left(-\int_0^L \sigma(\lambda, T) \cdot N(l) dl\right) \tag{7}$$

where

λ = *wavelength* (m)

L = *path length* (m)

dl = *incremental path length* (m)

σ = *absorption cross section* (dimensionless)

N = *molecule number density* (m^{-1})

T = *temperature* (K)

Two simplifying assumptions are made to Equation 7 for the current application. First, the absorption cross section, which is a function of temperature and wavelength, was assumed to be just a function of wavelength. Second, since the OPRS was used in relatively short range and constant altitude applications, the oxygen number density was assumed to be constant over the path length. It is important to note that these two assumptions were made to reduce the effort in the data analysis process, and are not required for using this method for range estimation. A straight forward method has been developed to estimate the concentration as a function of the distance along the line of sight (Hawks, 2006). This method assumes an exponential atmosphere and solves for the concentration path length at long ranges by using the first 11 terms of an infinite series. These assumptions result in Equation 7 simplifying to

$$\mathcal{T}_{O2}(\lambda, L) \approx \exp\left(-\sigma(\lambda) \cdot N \cdot L\right) \tag{8}$$

After applying Beer's Law in a monochromatic fashion by performing this exponential, the spectral transmission was convolved with the band pass filter and then normalized by the filter bandwidth which resulted in total transmission as a function of the length used:

$$\mathcal{T}_{O2}(L) \approx \int \mathcal{T}_{Filter}(\lambda) \cdot \mathcal{T}_{O2}(\lambda, L)\, d\lambda \tag{9}$$

This process was then repeated with different path lengths and combined to develop a metric curve of oxygen transmission versus path length (Figure 3). This curve was developed assuming standard temperature, pressure, and no humidity. Since the actual test conditions were not standard, this relationship required correction prior to comparing

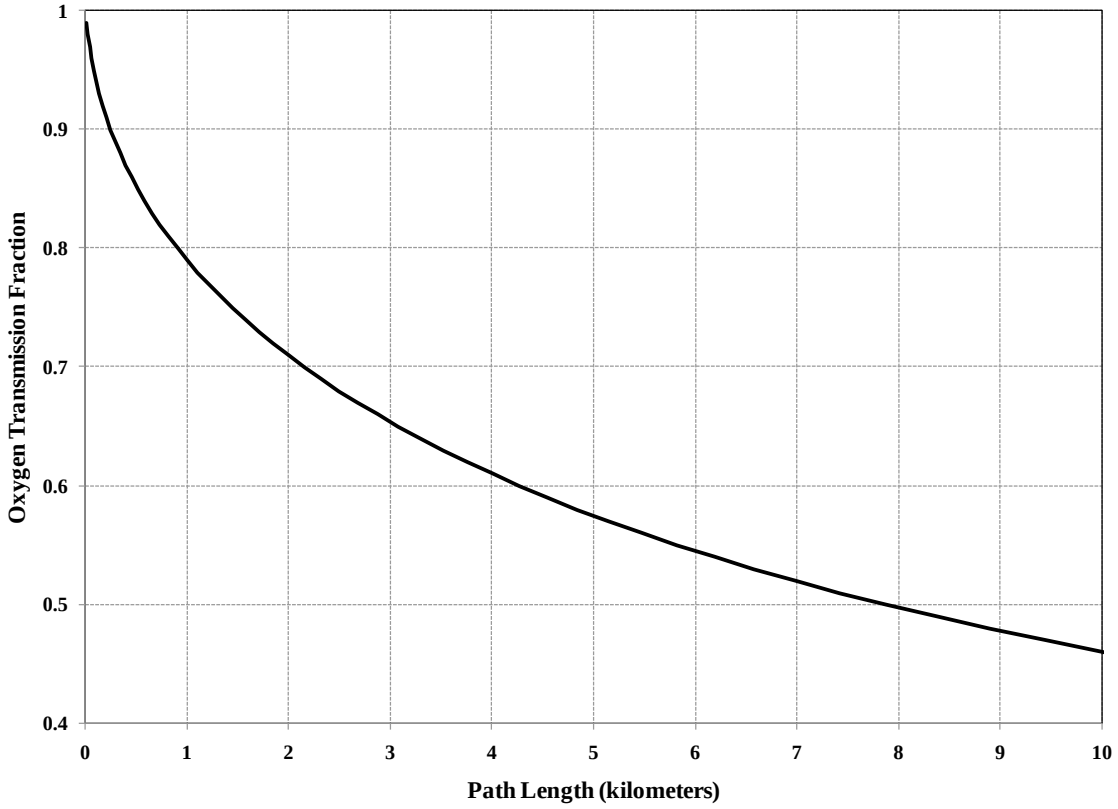

Figure 3. Transmission Prediction of the Path Length for the OPRS

values from the measured transmission. The humidity in the air displaces oxygen molecules and must be accounted for to accurately estimate the oxygen number density. One process to account for this change is to combine the humidity and the temperature into a single virtual temperature that incorporates the effect of humidity on number density into the temperature (Hawks, 2006). As the temperature and pressure change, the number density of the oxygen molecules also changes according to the ideal gas law.

Reviewing Equation 8 shows that the number density and the path length have a linear relationship. While holding the transmission fraction constant, an increase in the oxygen number density would require a linearly proportional decrease in the path length. Therefore, an increase in the number density can be accounted for by a proportional reduction in the estimated path length. These changes to the number density are then accounted for by using a ratio of the pressure and temperature to correct the path length for a given transmission factor as shown here:

$$L_{Corrected} = L_{STP} \cdot \frac{T_{Virt}}{300\ K} \cdot \frac{1\ Atm}{P_{Act}} \tag{10}$$

where

L_{Cor} = *corrected path length* (m)

L_{STP} = *original path length* (m)

T_{Virt} = *virtual temperature* (K)

P_{Act} = *actual pressure* (ATM)

This modified path length vector can now be used with the original model transmission factors to create the oxygen transmission versus path length curve corrected for the test day conditions. The measured transmission calculated previously is then compared to this curve to determine the range estimate.

System Description

The OPRS consisted of multiple pieces of equipment which worked together to collect images that were used to estimate range. The sensor was a Princeton Instruments PI-MAX® 512-T, Generation IV ICCD camera which was able to image in the 500-865

nm range. This camera had a gallium arsenide photocathode and a micro-channel plate capable of providing an electric potential of up to 1.2 million electron volts, or 255 gain, for image intensification. The sensor array was 512 by 512 pixels, but was operated using binning so that there were 256 by 256 effective pixels. A camera control unit provided power to the camera as well as an interface to the laptop computer (via universal serial bus) which operated the camera using the LabVIEW software. The camera was fitted with an 80-200 millimeter manual zoom lens which resulted in a field-of-view of 3.5 degrees to 8.8 degrees. The lens aperture was adjustable from an f-number of 2.8 up to 22. A Cambridge Research Institute SNIR-20 liquid crystal display (LCD) band pass filter was attached to the front of the zoom lens. This filter was tunable at 10 Hertz from 650 to 1100 nm and each filter setting had a full width half maximum of 5 to 7 nm. A filter control box interfaced between the LCD filter and the laptop computer. LabVIEW code developed as part of this thesis enabled coordination of filter settings and camera imaging. This code started the camera at the 778 nm band pass setting, took an image and waited the integration time. The software then commanded the filter to the next setting while reading, recording, and displaying the image to the computer. An additional time delay was entered into the system to allow the filter to completely stabilize. Figure 4 show a diagram of the camera and filter with a timeline indicating the sequencing of the image collection process. The images were recorded in 16 bit tagged image file (.tif) format with a time stamp provided by global positioning system time. The camera was capable of imaging roughly six frames per second for the conditions of this test. A set of three consecutive images was required to make a single range estimate.

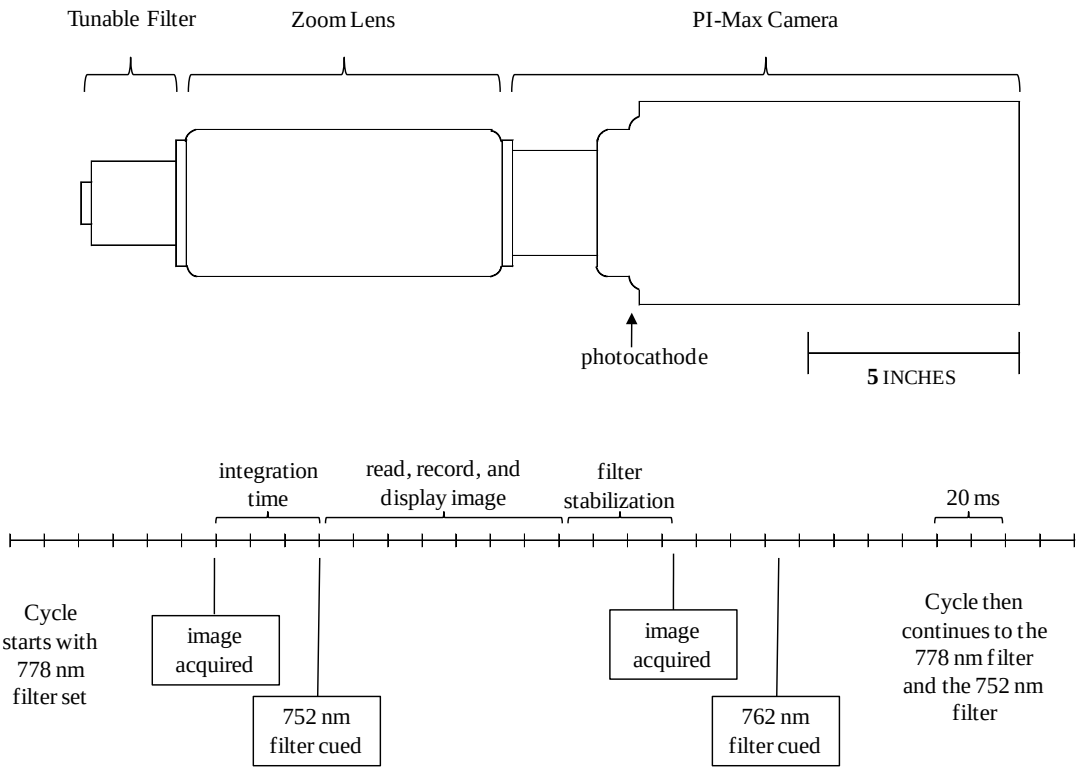

Figure 4. Schematic of the OPRS Sensor and Timing Cycle

The OPRS was modified for use both on the ground and in-flight mounted in a C-12 aircraft.

Image Analysis

The image analysis process to determine the signal measurement from each frame varied for stationary and moving targets. All frames had a non-uniformity correction applied as described in Appendix A. For the stationary targets, the hottest 1 to 100 pixels around the source were evaluated to determine the set which had the highest signal to noise ratio. This set of pixels was then averaged and used to calculate the signal value for all images. The background value from these pixels was then subtracted out to determine the signal measurement for each frame. For the moving target, the single hottest pixel

from the target was used to determine the signal measurement. The background value was estimated based on the surrounding pixels, and was then subtracted from the hot pixel to determine the signal value.

Experimental

The OPRS was developed and initially tested at AFIT in October 2008. The initial tests used two different sources, a halogen shop lamp and an incandescent flashlight. These tests were accomplished at ranges between 50 meters (m) and 380 m. The OPRS functioned well and the measurement error varied between less than 1% and 26%, with an average error of 12%. The OPRS was then taken to the USAF Test Pilot School (TPS), Edwards AFB, CA for tests using an F-16 aircraft in afterburner for the target as shown in Figure 5. Testing was accomplished as part of the Class 09A Air Cyclops test management project (Anderson and others, 2009). The OPRS was tested on the ground using a static F-16 and was then installed in a C-12 aircraft for airborne testing. This was the first test of the OPRS against an operationally significant target.

Figure 5. OPRS Ground Test Set-up and F-16 Target

Ground Test Set-Up

The OPRS ground test was conducted on 2 September 2009 from 2030 to 2330 hours local time. The F-16 (with an F-110-GE-100 engine) was secured to a thrust stand at the edge of Roger's dry lakebed and the OPRS was set up in a mobile fashion as shown in Figure 5. The OPRS system recorded filtered images of the F-16 afterburner plume from the lakebed at the locations indicated by stars in Figure 6. Images were recorded at a rate of 6 per second. The result for each run consists of the average of approximately 300 separate range estimates. An initial calibration run was used to optimize the OPRS settings prior to the actual test runs. Data were collected for three minutes at each location. The atmospheric conditions for each run are recorded in Appendix B.

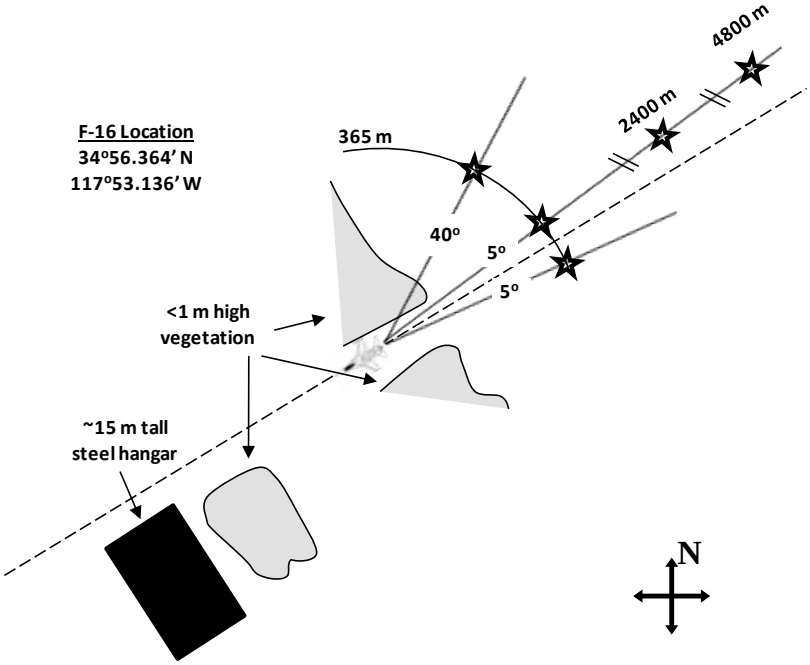

Figure 6. OPRS Ground Test Site Survey

Ground Test Results

The results from the ground test are shown in Figure 7 and are plotted with the model predicted transmission. Range errors averaged 15%, and were plotted against

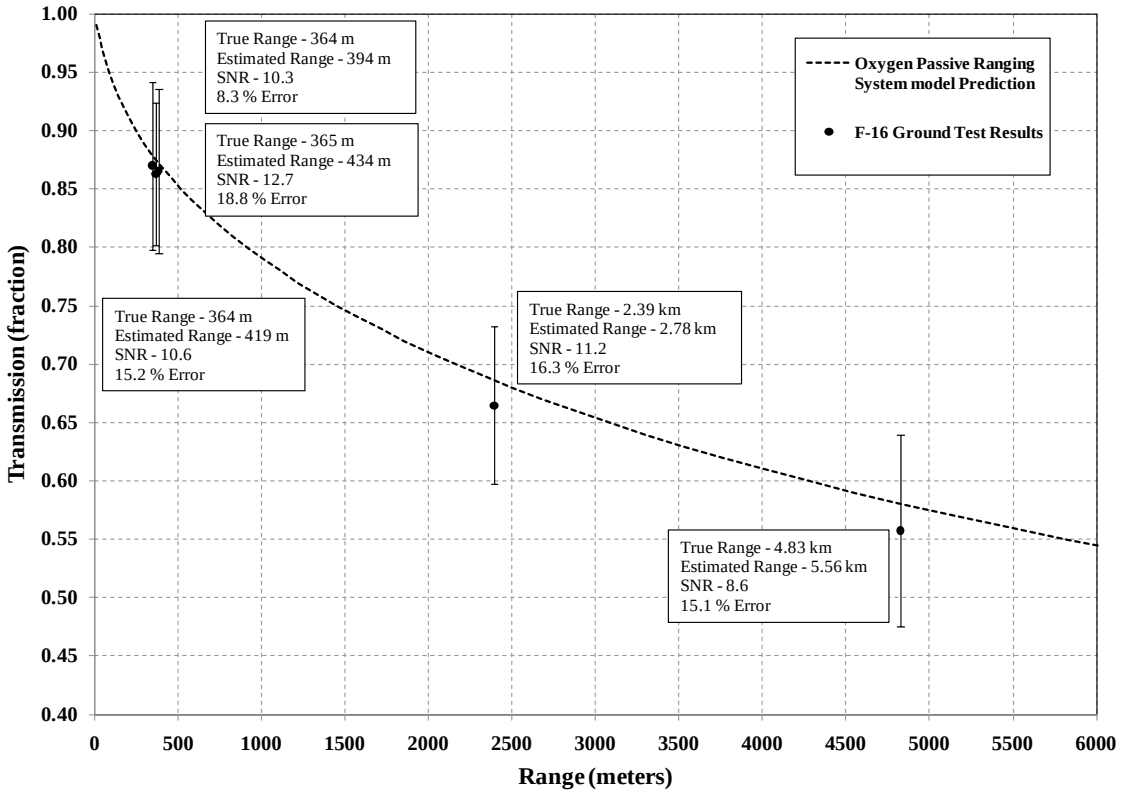

Figure 7. OPRS F-16 Ground Test Results

many variables including look angle, absorption, range, and SNR. No strong correlations existed between these variables and range error. While the model predictions are near the center of all of the error bars, the uncertainty was very high due to the low SNR values. The transmission uncertainty was in the range of 6% - 8% for all test points. Range uncertainty, which was derived by evaluating the transmission uncertainty on the metric curve, was even higher and varied from - 40% up to 125%.

There are several possible sources for this high uncertainty. The first is the camera itself. Figure 8 shows the signal measurements for each filter band pass, as well as the corresponding averages. The first thing to note is the signal measurement variations with time. All three band pass filters are affected by the camera response.

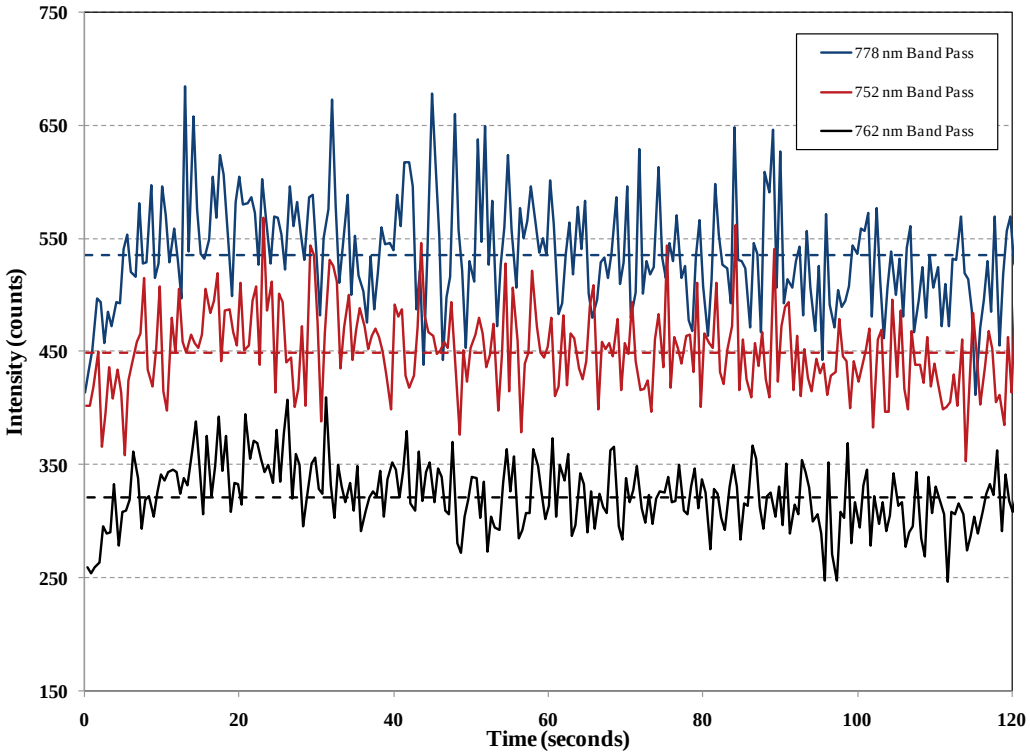

Figure 8. OPRS Sample Signal Measurements from the F-16 Ground Test

The signal levels start low, and then rise and fall over the three minute test. This is the first indication that the camera is not providing consistent data. This signal has both low frequency small amplitude content as well as high frequency large amplitude content. This trend had been seen in earlier tests, and was not just due to changes in the afterburning plume. Although these low frequency variations in signal intensity generally correlate well between band passes, the high frequency content does not always correlate within the same range estimate. Figure 9 depicts the intensity of the 762 nm signal plotted against the 752 nm signal. This shows that there is some correlation between bands, but the correlation is not strong. This low correlation resulted in large variations in transmission calculations as can be seen in Figure 10, which shows the transmission plotted on the left axis and the range plotted on the right axis. Since the

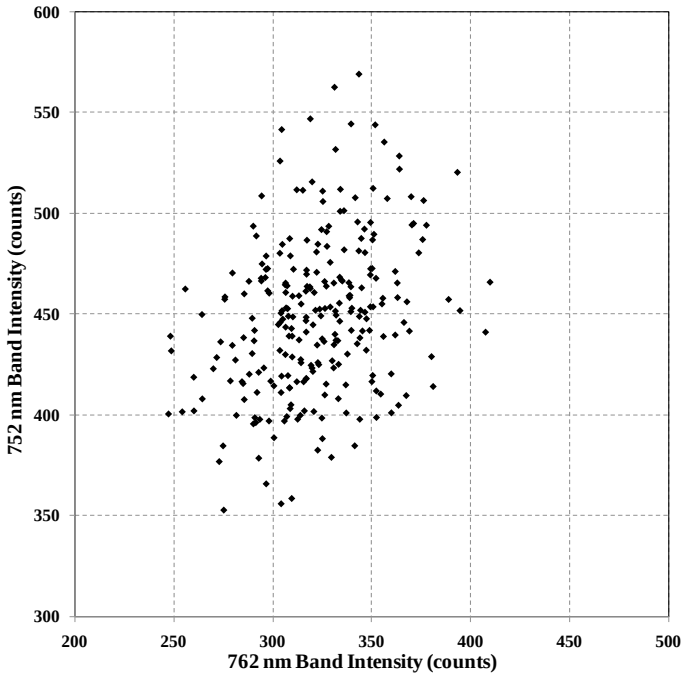

Figure 9. Correlation Plot of the F-16 Ground Test Data

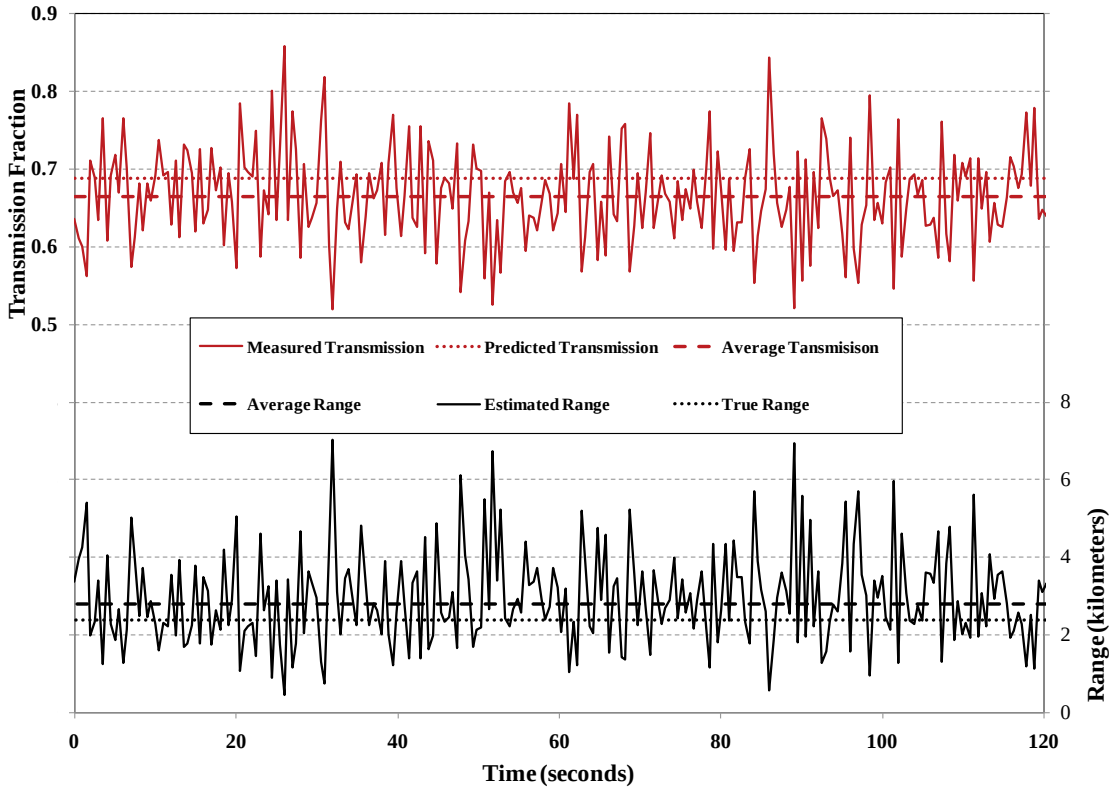

Figure 10. OPRS Transmission and Range Estimates for the F-16 Ground Test

OPRS took band pass images serially (one at a time), variations in the noise caused signal variations between band passes. A system capable of capturing all three images simultaneously would eliminate noise variations within each independent range estimate. Besides camera response variations, the serial imaging caused additional uncertainty due to the variations in the source intensity over time. Random fluctuations in the target intensity due to turbulence or the flickering of the afterburner also added noise between frames.

Figure 11 shows a sample of six consecutive OPRS images. The red color indicates a high signal level and the blue indicates a low signal level. The signal ranges from 52,000 counts as the hottest pixel in the 778 nm image, and 100 counts being the cold background pixels in all of the images. These images show that the basic shape of the hot region remains the same, but that slight signal variations do occur with time.

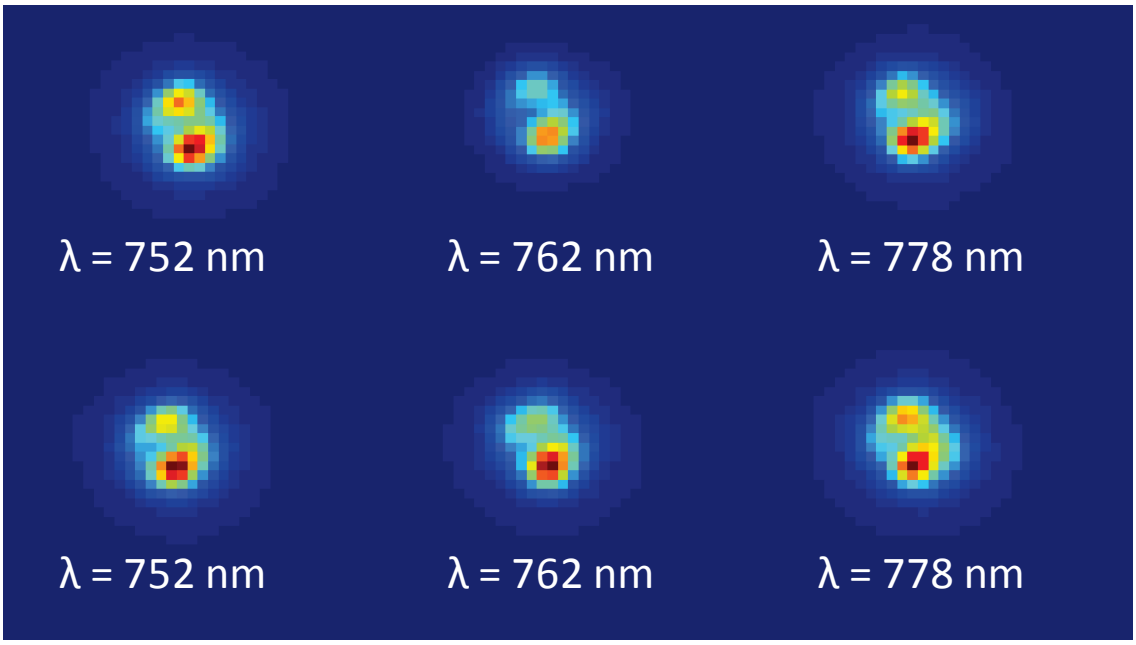

Figure 11. OPRS Images of F-16 Afterburner During Ground Testing

The combination of these variations in signal resulted in a low SNR and therefore large uncertainties. The SNR was determined by taking the average signal intensity and dividing that by the standard deviation of the signal intensity. The effect that SNR had on the uncertainty was mathematically estimated by taking the 300 independent range estimates from a single run and randomly selecting a set number of data points which were averaged to determine a transmission estimate. This was then repeated one hundred times to generate a vector of signal intensities and a vector of transmission estimates. The SNR of the signal intensity was then recorded with the corresponding standard deviation of transmission values. This process was then repeated changing the number of data points averaged, and the entire process was repeated using each data set. The resulting SNR values and transmission uncertainties were plotted and fit to the curve shown in Figure 12. A similar analysis was performed for the atmospheric oxygen passive ranging system (Hawks, 2006). The data was fit to an exponential of the form $y=\left(C_1/\sqrt{x}\right)\exp\left(-x/C_2\right)$ which had the characteristic of uncertainty approaching zero as the SNR approached infinity, and the uncertainty approaching infinity as the SNR approached zero. The fit to the previous work had $C_1 = 73.3$, and $C_2 = 1{,}052$. In Figure 12, $C_1 = 0.229$, and $C_2 = 46.2$. The fit from Hawks' work is therefore shifted up and to the right of the current results.

Overall, this shows that for the current system with SNR values around 10, the transmission uncertainty is around 7%, which results in a large range uncertainty as discussed previously. This plot also shows that for a modest improvement of SNR to 50, the transmission uncertainty is reduced to 1%, which, for these ranges is a more reasonable range uncertainty (roughly 10%). Therefore, although the current system has

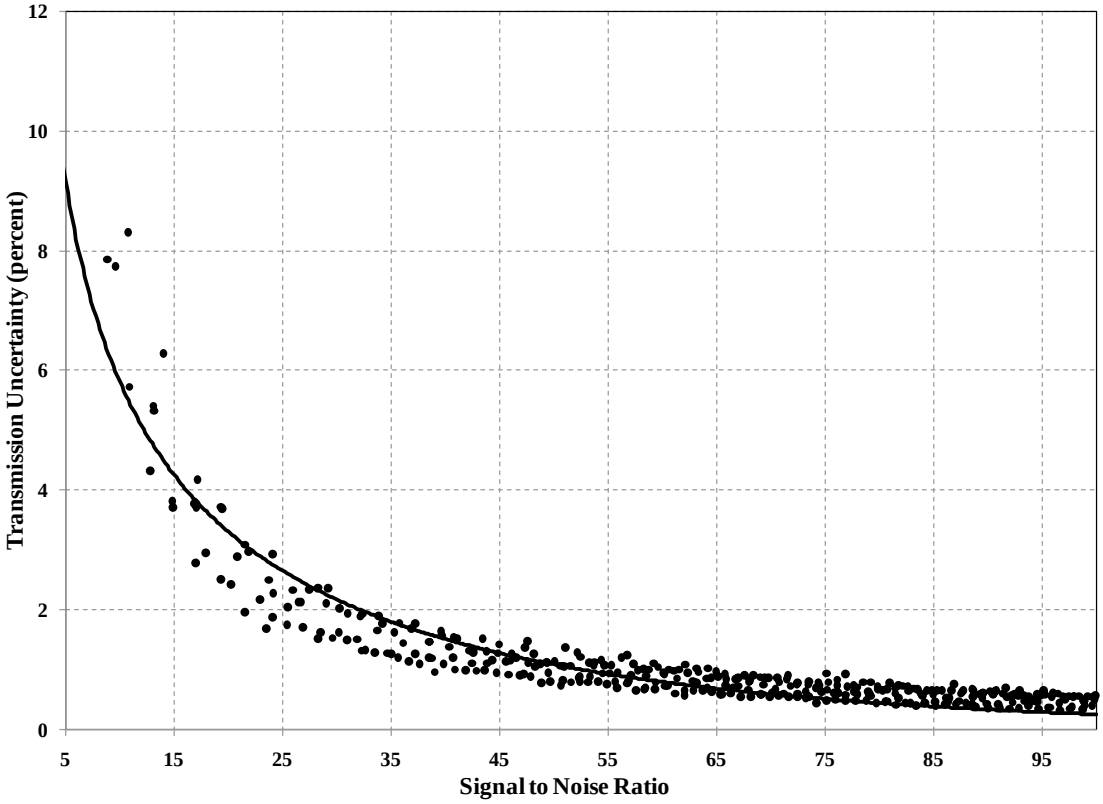

Figure 12. Signal to Noise Ratio Effect on Transmission Uncertainty

a large uncertainty, a small improvement in the measurement noise can yield a great effect on the repeatability of the system.

The atmospheric conditions were measured at the sensor and could have varied along the path to the source. This adds additional uncertainty that is associated with the measurement of temperature, pressure, and dew point (used for the humidity measurement). This was characterized by changing their input values by some arbitrary amount in the calculations to note the response this had on the transmission estimate. These effects are documented in Table 1. The transmission uncertainty varied with range, so the effects were documented for each of the ranges used in the test. The transmission estimate was not very sensitive to any of these errors. The highest of all

Table 1. OPRS Transmission Uncertainty Due to Atmospheric Measurement Errors

	Transmission Uncertainty Due to Following Measurement Errors (%)					
	Temperature Error		Pressure Error		Dew Point Error	
Range (km)	+2˚ C	-2˚ C	+5 mBar	- 5 mBar	+5˚ C	-5˚ C
4.83	-0.11	0.10	-0.03	0.02	0.08	-0.09
2.39	-0.09	0.09	-0.02	0.02	0.07	-0.07
0.36	-0.04	0.05	-0.01	0.01	0.04	-0.03

these transmission uncertainties is 0.11%. Compared to the transmission uncertainty due to the SNR of roughly 7%, this is negligible. This is also an important result because it shows that a precise atmospheric characterization is not necessary to produce good range estimates with this method. It was also noteworthy that none of the range estimates were shorter than the actual range. The range errors were all between 8 percent and 21 percent. This indicates a possible systematic error in the range calculation. Due to the combination of the large error bars and the limited amount of data collected with the OPRS, however, it is difficult to conclude whether or not a systematic error does exist.

Despite the several data quality issues, the OPRS was able to estimate the range to the F-16 afterburning plume. There are several enhancements that can be incorporated, but the current system was able to estimate range to an afterburning jet plume with an average range estimation error of 15%.

Flight Test

Flight testing was accomplished from 14 to 23 September 2009 at ranges varying from approximately 200 m up to approximately 13 km. The C-12 carried the OPRS for the flight test, and the F-16 afterburner jet plume was the target (Figure 13). Look angles

Figure 13. OPRS Flight Test Set-up

to the target varied horizontally as well as vertically through the atmosphere. The C-12 was in straight and level flight at 9,500 feet pressure altitude with the Lexan© door open and the OPRS imaging through the opening. The outside air temperature was 11˚C. The target aircraft flew away from the left side of the C-12 in afterburner while a camera operator manually tracked and imaged the afterburning exhaust with the OPRS. All flight testing was executed during daylight conditions, and there was significant background illumination.

Image analysis was performed using a variety of manual methods to extract some relevant range information from the flight test data. The method that was used took the value from the hottest pixel of the afterburner from each frame to estimate range. The signal levels and truth range results using this method can be seen in Figure 14. This method had faults, which will be discussed, but was the most consistent of the data analysis techniques attempted. Other methods attempted were to use the entire frame, and subtract an estimated background level, and also to manually select an area around the afterburner which was believed to include the entire signal. While the latter method is believed to be the most accurate, it was highly subjective, and not repeatable. Using

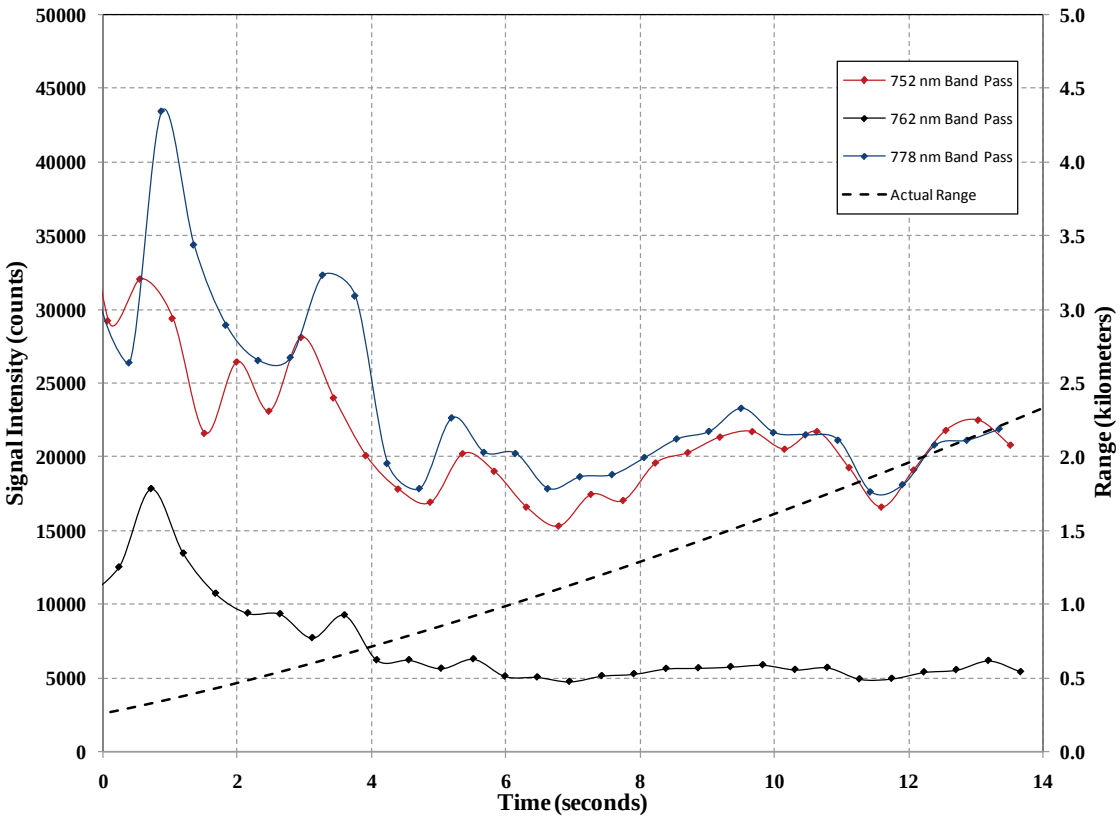

Figure 14. OPRS Signal Measurements from the Flight Test

the method described previously, the OPRS was not able to provide a consistent or accurate range estimate. The OPRS range estimates are shown in Figure 15. Two sets of data are plotted. The first is the collection of all images regardless of image quality, and the second contains only the range estimates from the images with a clear image of the F-16 afterburner section. The images collected appeared to have valid signal levels, as determined by the high intensity signal from the exhaust nozzle. The recorded images also showed that the overall intensity decreased with range. These observations indicated that the emitted afterburner signal, and not just the reflected sunlight, was recorded. Images at a range of 500 m for each consecutive band pass filter (752 nm, 762 nm, and 778 nm) are shown in Figure 16. Each image was obtained approximately 150

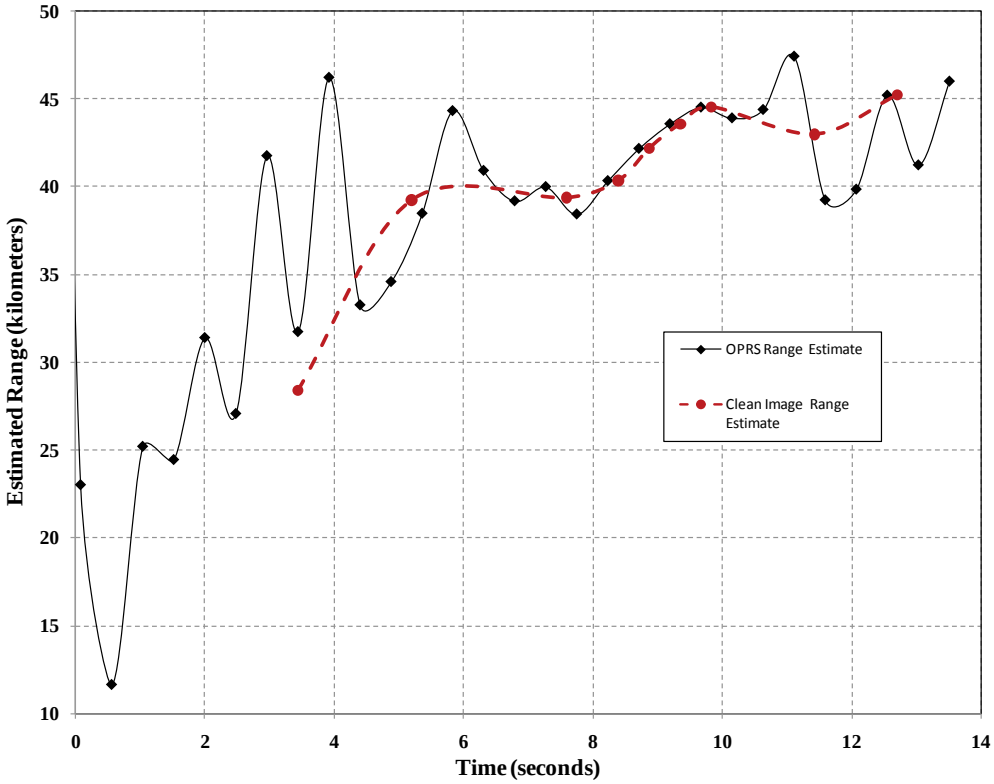

Figure 15. OPRS Range Estimates from the Flight Test

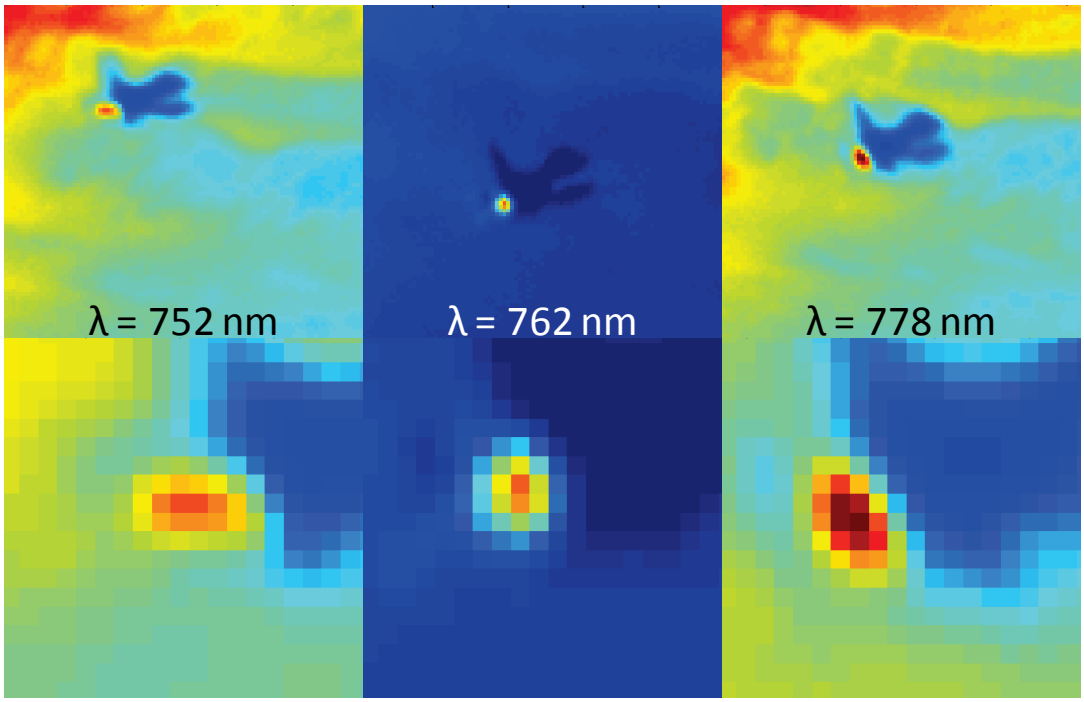

Figure 16. OPRS Images of F-16 from the Flight Test

milliseconds apart. The red color indicates a large signal value and the blue color indicates a small signal value.

Although this test did not yield valid results for the OPRS accuracy in flight, there were several important things learned from the flight test that should be considered for further dynamic testing of passive ranging systems. The background clutter, the serial imaging, the data analysis process, and the solar reflections are the main contributors to the poor performance of the OPRS in flight and were not properly addressed with this system.

The serial imaging of the OPRS has already been discussed as it relates to a stationary target, namely that the camera response and afterburner plume are changing with time. Those issues continue to plague the system in the dynamic environment, and are even more problematic since the errors cannot be reduced by time averaging. In addition to this, however, the serial imaging of the band passes increases the difficulty in accomplishing both the background subtraction and the data analysis. One other minor error induced from serial imaging was that the target was at a different range for each successive image. It was expected that this error could be minimized by fitting the data points to a curve and then estimating range at the same point in time based on the fit of the data, but due to the low SNR and additional errors explained below, the data were not consistent enough to use this method to produce repeatable range estimates.

The data from the 752 nm and the 778 nm band pass filters showed that there was significant background signal present. It can be seen in Figure 16 that some of the background signal was even near the same intensity as the F-16 nozzle. Since the target was moving and the background was continuously changing, it was impossible to acquire

a background image of the same airspace the target was passing through. This made it extremely difficult to account for the background signal. The serial imaging increased the difficulty of this background subtraction since each of the three frames required for a single range estimate now had different backgrounds, which were each estimated separately.

The OPRS data analysis process used manual target recognition and resulted in repeatability errors in measuring the actual signal for the flight test. For the ground test, the target size used was determined by evaluating different sized areas around the target, then using the target size that maximized the SNR. This works for a stationary target, but cannot be accomplished when analyzing a moving target. This was complicated again by the serial imaging due to the varying levels of signal blurring. As the camera was tracking the F-16, some images were blurred by camera movement, while others were clear because the camera was relatively stationary. This resulted in signal from the F-16 sometimes being focused into a few image pixels, while other times, the signal from one image was blurred across many image pixels. This can be seen by again referring to Figure 16. The plume in the 752 nm band pass image has a horizontal oval shape, the plume in the 762 nm band pass image has a circular shape, and the plume in the 778 nm band pass image has a near vertical oval shape. The actual shape of the plume was not changing, but the camera, as it moved to track the F-16, captured a slightly different image depending on the camera movements at the time of exposure. The target recognition process eventually used for the flight test was to just evaluate the hottest pixel on the target and use that as the entire signal. This was inadequate and the flight test data

need to be re-evaluated with automated target recognition algorithms to potentially extract some valid range estimates.

One final observation from the flight test was the effect of solar scatter and reflections. This is something that will be problematic for a wide variety of passive ranging systems. Any scattered light that enters the OPRS from the sun will result in range estimates that are long, due to the solar light having a path length through the thickness of the atmosphere. Solar reflections can also be problematic. Passive ranging devices are typically trying to range something that is man-made and reflective such as metal. It was noticed several times during the flight test that solar reflections from parts of the F-16 were brighter than the afterburner signal. Solar reflections from glass or water surfaces on the ground will also cause this problem. For this test, it was clear these were solar reflections, and it was only a minor annoyance. For an automated system that is seeking new targets, however, those would be new targets. The real problem is that systems do get fielded with this type issue, and the distractions to the operator many times outweigh the perceived benefits and they simply turn the system off.

Conclusions

The USAF TPS test results showed that the OPRS was able to estimate range to a militarily significant target at ranges up to 4.8 km. The range errors varied from 8 to 21 percent. The OPRS proved to work according to theory during the ground tests and means that band pass filtering can be used to measure atmospheric oxygen absorption to passively determine the range to an emissive target. The additional complexity of air to air ranging, with a multitude of additional variables to the signal proved to be too

problematic for the system, and the OPRS was unable to accurately estimate range to the airborne F-16 target.

In its current state, the OPRS is not a viable solution to the passive ranging problem, but several potential improvements were identified that could make it militarily useful. First, the signal noise was too high. The SNR values of 8 – 12 for this system were prohibitively low for the system to be useful. Second, the band pass images need to be recorded simultaneously to ensure correlation between images. Last, the data analysis process needs to be automated to accurately and repeatably estimate the signal for each image. Two other items that will be problematic for any passive ranging system are solar reflections and determining the background signal for a constantly changing background. These two items do not seem to be prohibitively difficult, but will take effort to develop a solution.

Passive range surveillance could be employed in concert with a multitude of other sensors to provide a stealthy means of target detection and ranging. It is a low energy and potentially low-cost solution to the covert ranging problem, but continues to be a difficult problem to solve. The solution is, however, now one step closer.

IV. Additional Testing

In addition to the F-16 testing that occurred as part of the USAF Test Pilot School project, there were two other tests accomplished with the OPRS. The first was the initial AFIT testing of the system at Wright-Patterson AFB, OH in October 2008. The second was in the desert at Edwards AFB CA, in January 2010. This chapter documents the results and findings of these additional tests.

Initial AFIT Testing

The initial AFIT test was accomplished in the parking lot and the grass field just east of AFIT. Testing occurred on October 9th and the 19th between the hours of 2100 and 2330 local and was accomplished using both a halogen lamp and an incandescent flashlight as the target source. The target was imaged for a total of two minutes at each location. The results are shown in Figure 17. The average range error was 12% and all range estimates lay within the error bars, which was consistent with the F-16 results. Some of the other notable results are that the SNR value varied considerably between test points. The two shortest ranges had fairly high SNR values (73, and 93) while the other test points had SNR values much lower (between 13 and 39). There is some trending for SNR to decrease with range, but there is too much variance in the SNR values to confidently draw that correlation. Also, there appears to be some correlation between the range and the range error for this data. At the 50 m and 103 m ranges, the OPRS underestimated the range, and at all the other ranges, the OPRS overestimated the ranges.

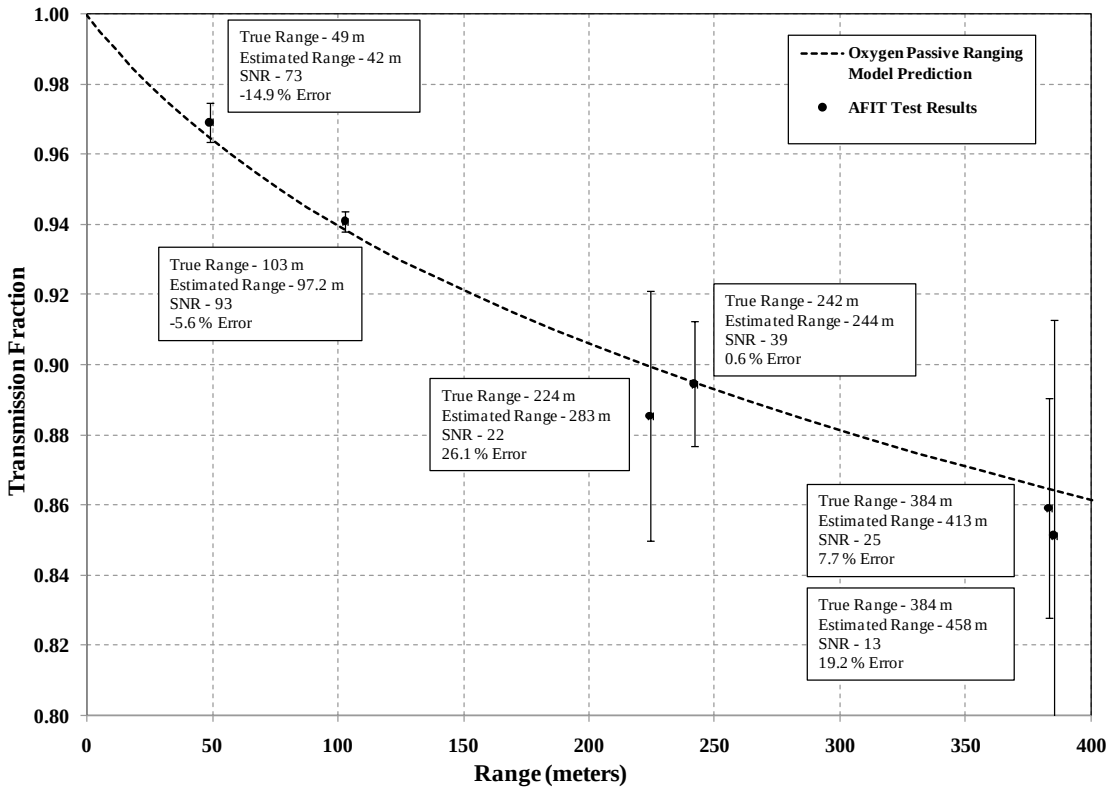

Figure 17. OPRS AFIT Ground Test Results

This was only partially consistent with the results of the F-16 tests. While all of the F-16 tests did overestimate range, the error did not increase with an increasing range.

Desert Tests

Neither the AFIT tests nor the F-16 ground tests were accomplished during daylight hours. Therefore, one final test set was accomplished during both hours of light and darkness. These tests were accomplished on January 2nd and 7th all at the same range of 534 meters. The target source was an incandescent flashlight and was imaged for five minutes. Two tests were accomplished in daylight and the other six were accomplished in darkness. The results are shown in Table 2. The average error for this test was 22%, which was higher than both the AFIT and the F-16 tests. The SNR values for this test

Table 2. OPRS Desert Test Results at 534 Meter Range

Run #	Day/ Night	SNR	Measured Transmission (%)	Transmission Error (%)	Transmission Uncertainty (%)	Estimated Range (m)	Range Error (%)
1	Day	10	84.3	-0.1	8.8	537	0.5
2	Day	15	86.5	2.5	6.2	403	-24.5
3	Night	7	80.7	-3.9	11.6	771	44.4
4	Night	12	81.4	-3.0	7.8	712	33.4
5	Night	9	84.8	0.6	9.7	498	-6.8
6	Night	4	83.0	-1.5	15.8	618	15.8
7	Night	4	85.7	1.7	15.4	441	-17.4
8	Night	6	81.5	-3.2	12.8	722	35.3

were in general much smaller than either of the previous tests, and this resulted in much larger errors and much larger error bars. Still, all of the estimated ranges fell within the error bars. The average of the eight range estimates was 588 m (10.1% error), with a range uncertainty of ± 139 m. This test showed that the OPRS was able to range in daylight conditions as well as in darkness. The SNR values were in general higher during the day than they were at night. On average, the OPRS still overestimated range, but three of the eight runs underestimated range indicating no strong likelihood of a systematic error.

Summary

Overall, the results of the AFIT and the desert tests correlated well to the F-16 tests. The OPRS was able to estimate range to both incandescent and halogen sources using only a limited amount of atmospheric data. The average range errors for each test

were between 12% and 22%. At all ranges over 200 meters, the OPRS in general overestimated range, but the error did not grow with increasing range. The low SNR values and the high uncertainty values resulted in making it difficult to draw strong correlations between range error and any test variables.

V. Conclusions and Recommendations

Passively determining range to targets is a current and continuing military requirement. To fill that need, an oxygen passive ranging system (OPRS) was developed that uses band pass filters with an optical camera to estimate the atmospheric oxygen transmission from an emissive target. A method was also developed to correlate that transmission to model predictions using the temperature, pressure, and dew point information collected at the detector to estimate the range to the target. This system was developed at the Air Force Institute of Technology (AFIT) and tested against halogen and incandescent light sources. The OPRS was then taken to the USAF Test Pilot School and installed on a C-12 aircraft. The OPRS was tested against an F-16 in afterburner during ground and flight tests.

Conclusions of Research

An oxygen passive ranging system was designed, built and tested. This system operated as designed and was able to capture data images of targets while operating in a static environment on the ground as well as in the highly dynamic environment of flight testing. These images were then processed and the data was compared to model predictions. This comparison resulted in range estimates that had an average range error of 15%. There were two major drawbacks of the OPRS. The first was the signal to noise ratio of the measurements. This resulted in long test runs to enable time averaging and also resulted in large error bars on the range estimates. This made it difficult to draw strong conclusions about the OPRS except for its overall accuracy. The second major

drawback of the OPRS was the serial imaging. The OPRS required three images using three different band pass filters to make a single range estimate. The OPRS acquired these images one after another roughly 150 milliseconds apart. The problem with this was that due to minor variations in signal intensities, the three images were not of an identical source. This was exacerbated in the flight test. When imaging a dynamic target serially, each of the three band pass images was vastly different. Overall, the research was a success and validated the theory of passive ranging using band pass filters to measure the atmospheric oxygen absorption.

Significance of Research

Although the current form of the OPRS is not a viable solution to the passive ranging problem, there were several significant findings in this research. The first is that it is possible to use properly designed band pass filters to measure the depth of the oxygen absorption feature near 762 nm. Prior to this research, this, and other absorption features had been measured by large and expensive spectrometers. This is important because it enables the use of much smaller and cheaper equipment. This leads to another significant finding. This homemade passive ranging system was shown to be robust enough that it could be easily installed onto an aircraft platform and function as designed. The importance of this is that the research shows the technology is at a level that can enable the theory and ideas of the OPRS to be implemented into a design that could be used in a real world scenario.

Recommendations for Future Research

This passive ranging system was shown to work, but needs improvement. Future research that can be performed is to build a system that makes the improvements called for in this thesis. The first improvement is to use a camera with a much higher signal to noise ratio. Although time averaging shows the capability of the system, a high SNR system is required to draw strong conclusions about this research and get statistically significant results. The second improvement is to create a system that takes three images simultaneously. This will also enable much better correlation between band passes and improve the data quality. A final area of future research is to optimize the filter band passes used to estimate the transmission fraction. The current system is only designed for target sources that do not contain potassium impurities. Filter optimization would greatly improve its usefulness against rocket plume type targets for which this technology is desired.

Appendix A. Oxygen Passive Ranging System Calibration

This appendix outlines the procedures used for the non-uniformity corrections, the LCD band pass filter area normalization, and the camera spectral response calibration.

Non-Uniformity Correction

A camera non-uniformity correction was accomplished prior to each set of testing. This was accomplished by first recording five hundred images in a dark room with the lens covered. These images were averaged to determine the average dark current by pixel. Next, five hundred images of a uniformly illuminated blank projector screen were all recorded and averaged by pixel. The dark current previously measured was then subtracted from each cell in the matrix to determine the true signal matrix. Next, each cell in the true signal matrix was divided into the average of the true signal matrix, which was saved as the non-uniformity correction matrix. To apply this correction, after an image was imported into MATLAB, the dark current was first subtracted from each cell. The image was then multiplied by the non-uniformity correction matrix, and this resulted in the corrected image. Figure 18 shows the difference between a raw image, and a non-uniformity corrected image. In the raw image, small honeycomb shapes and small imperfections in the ICCD are visible in the center of the image. These imperfections are eliminated in the non-uniformity corrected image. Due to the vignetting of the LCD filter, the non-uniformity correction is not perfect. This is seen in the signal around the edges of the image. This was an additional source of error in the flight test, but was not an issue in the ground tests. This process was accomplished using varying camera

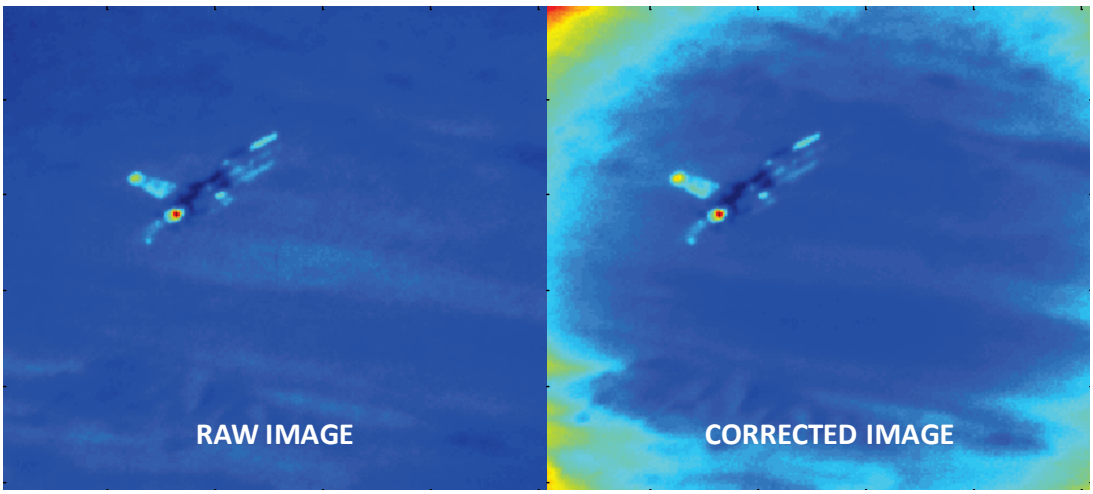

Figure 18. Raw Image and Non-uniformity Corrected Image

settings (gain, and integration times), but these settings made no significant difference in the non-uniformity correction that was applied to the images.

Filter Line Shape Measurement

The filter line shape was measured using an AFIT owned photo spectrometer. Each band pass filter was evaluated using this process, and the data points were fit to a Gaussian function as shown in Table 3. Each fit matched the spectrometer data with an R squared value of greater than 99%. This Gaussian line shape function was then used for the OPRS calculations.

Table 3. Tunable Band Pass Filter Fit Parameters

$y = a \cdot exp\ -[(x-b)/c]^2$			
Filter Band Pass (nm)	**a**	**b (nm)**	**c (nm)**
778	0.321	777.8	3.17
762	0.309	761.8	3.02
752	0.311	751.8	2.98

Camera Spectral Response Normalization

To evaluate the variation of camera spectral response, a calibrated blackbody was imaged using all three filter band passes at both 950° C, and 1200° C. The theoretical blackbody radiation curve was then mathematically convolved with each filter line shape and normalized to the 778 nm band pass signal level. The actual signal measured from each band pass was also normalized to the 778 nm band pass. The values from the theoretical measurement were then combined in a ratio with the actual values measured to determine the relative spectral response of the camera. This ratio was then applied to the raw measurements during the ranging calculations to determine the camera response corrected signal levels. Through this process, it was determined that a normalization factor of 0.913 should be applied to both the 752 nm and the 762 nm band pass signal to account for the variation in camera response.

Appendix B. Test Day Atmospherics

The following tables document the atmospheric conditions for each test run. Table 4 includes the data from the AFIT test, Table 5 contains the data from the F-16 ground test, and Table 6 includes the data from the desert test.

Table 4. OPRS AFIT Test Atmospheric Conditions

Date (mm/dd/yyyy)	Time (local)	Temperature (˚C)	Dew Point (˚C)	Pressure (millibars)
10/9/2009	2210	13.5	8.8	984.2
10/9/2009	2230	13.2	9.5	984.4
10/9/2009	2310	13.1	9.9	984.4
10/19/2009	2200	14.8	2.6	984.3
10/19/2009	2230	14.8	2.9	984.1
10/19/2009	2340	14.8	2.9	984.1

Table 5. OPRS F-16 Ground Test Atmospheric Conditions

Date (mm/dd/yyyy)	Time (local)	Temperature (˚C)	Dew Point (˚C)	Pressure (millibars)
9/2/2009	2115	29.3	9.2	932.8
9/2/2009	2140	29.5	7.6	933.0
9/2/2009	2200	28.8	7.6	933.2
9/2/2009	2250	27.9	5.8	933.0
9/2/2009	2310	28.3	4.6	933.2

Table 6. OPRS Desert Test Atmospheric Conditions

Date (mm/dd/yyyy)	Time (local)	Temperature (˚C)	Dew Point (˚C)	Pressure (millibars)
1/2/2010	1520	15.7	-3.9	935.8
1/2/2010	1550	15.6	-3.9	935.8
1/2/2010	1910	4.4	-6.1	937.3
1/2/2010	1930	2.1	-6.1	937.7
1/7/2010	1815	10.0	-2.8	933.2
1/7/2010	1825	10.0	-2.8	933.3
1/7/2010	1830	10.0	-2.8	933.4
1/7/2010	2150	7.4	-3.9	934.5

Appendix C. Data Acquisition and Analysis Programming

This appendix outlines some of the LabVIEW and MATLAB computer coding that was developed to create the oxygen passive ranging system.

Data Acquisition

LabVIEW software code was programmed to develop a means of interfacing both the Pi-Max camera and the tunable LCD filter as well as time coding and saving the data images to a computer hard drive. The software first initiated communications with the camera and the LCD filter, then sent the user specified camera settings to the camera and the initial band pass setting to the LCD filter. The program then began continuously taking images using these settings and displaying these images on the computer screen. The system remained in this cycle until the operator selected a start recording button. This began the cycle of taking an image, adding both a time stamp and a band pass stamp, recording the image to the hard drive, sending the filter a new band pass setting, waiting for the filter to switch, and then taking another image. This process was repeated roughly six times per second. The filter switching cycle went from the 778 nm band pass to the 762 nm band pass, to the 752 nm band pass, and then back to the 778 nm band pass. Figure 19 shows a screen shot of the input screen and Figure 20 shows a screen shot of the LabVIEW source code.

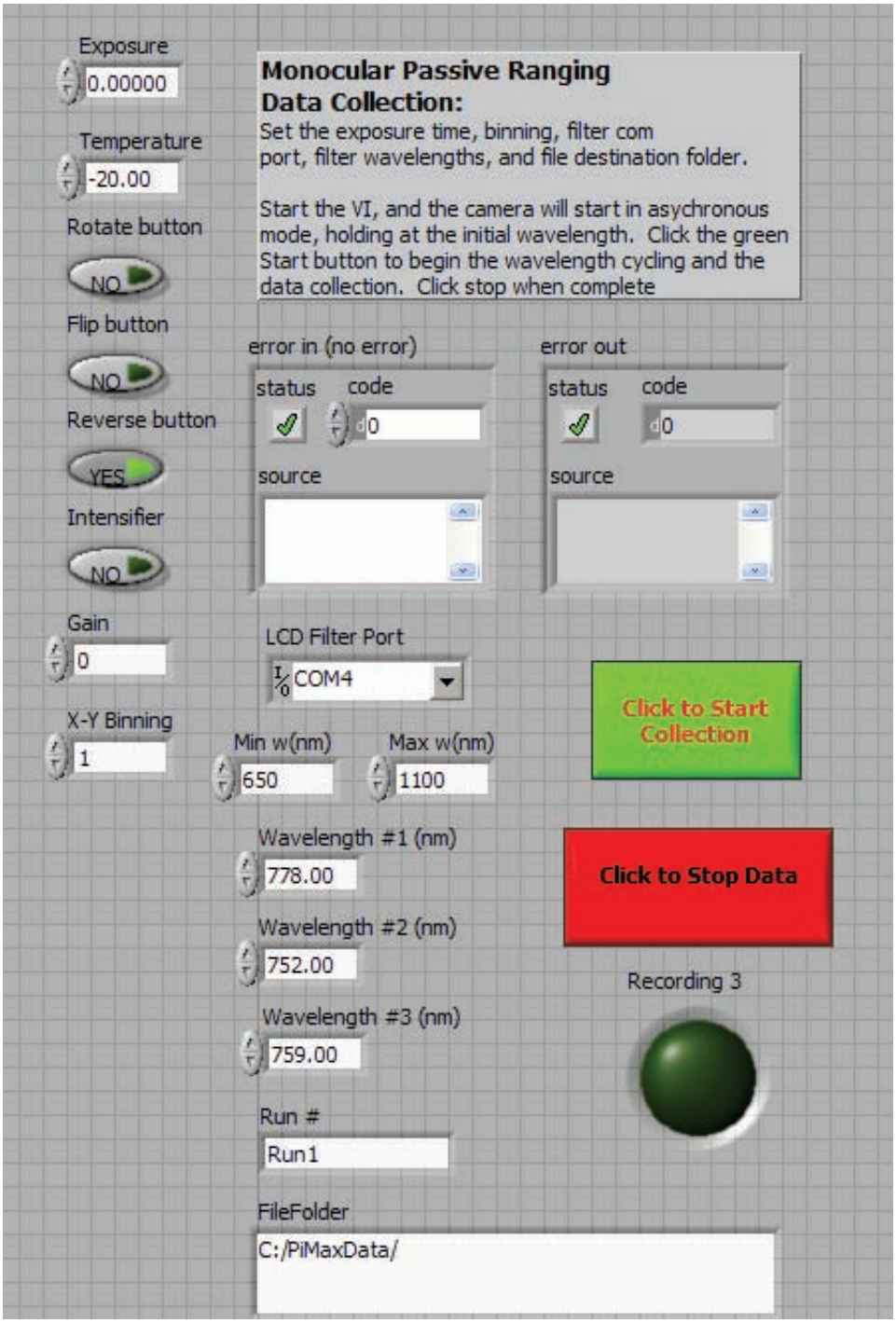

Figure 19. Screenshot of LabVIEW Input Code

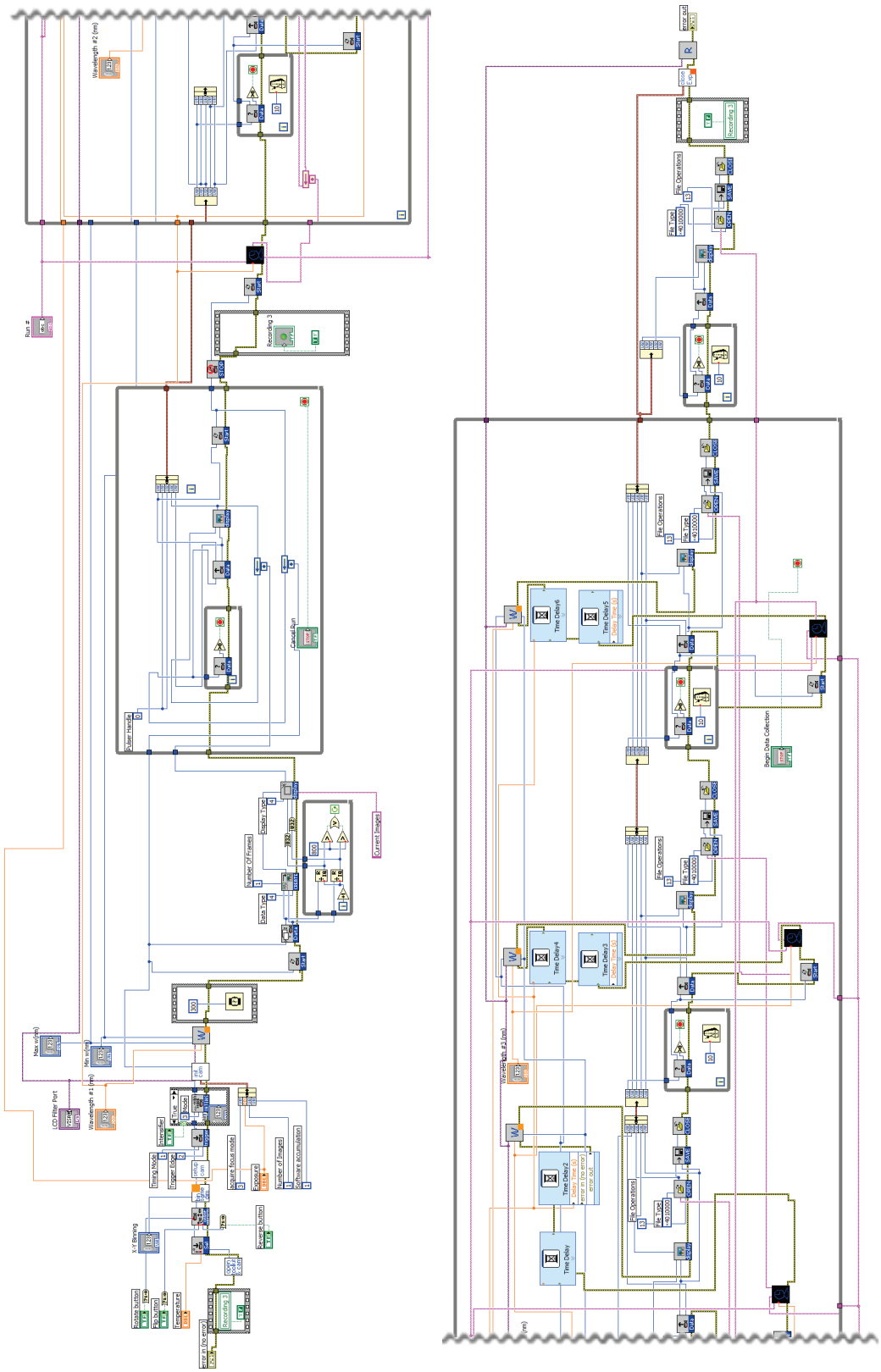

Figure 20. Screenshot of LabVIEW Source Code

Data Analysis

MATLAB was used to analyze and process the images to determine range estimates. Although the following sample of the routines does not include all of the information that is required to reproduce the results (databases, constants, subroutines), it does document the overall process of the data reduction.

This first section is the overall code which allows for entering the atmospheric conditions and file locations. This file then calls other subroutines which are shown below.

```
            Read LabView Files and Determine Range
%Fill out data and run entire file
binning=1;% 1x1 binning=1 and 2x2 binning=2
wavelength=759;% Enter 762 or 759 for absorption wavelength
run_num=1;
day_num=244;
folder='Data/EdwardsDayTest/RealRun1';
runst=num2str(run_num);
dayst=num2str(day_num);

xRange=333:342;%Range of Pixels to avg
yRange=262:271;

temperature=29.28;% in C
dew_pt=9.1667;% in C
pressure=932.8;% in mBar
if wavelength==762
    if binning==1
      %              1X1 Binning      762
     string1=strcat(dayst,'*WL778-RUN',runst,'.tif');
     string2=strcat(dayst,'*WL762-RUN',runst,'.tif');
     string3=strcat(dayst,'*WL752-RUN',runst,'.tif');

[m778,n778,m762,n762,m752,n752,t778,t762,t752]=read_labv(20
08,10,8,folder,string1,string2,string3,yRange,xRange);

        % Use average values
      a752=mean(t752);
      a762=mean(t762);
      a778=mean(t778);

      clear s778 s762 s759 s752;
        for i=1:length(n762);
            s762(i)=(n762(i)-n778(1))*24*3600;
        end;
```

```
        for i=1:length(n752);
            s752(i)=(n752(i)-n778(1))*24*3600;
        end;
        for i=1:length(n778);
            s778(i)=(n778(i)-n778(1))*24*3600;
        end;
        plot(s778,t778);hold all;plot(s762,t762);hold
all;plot(s752,t752);hold off; figure(gcf)

[transm,c762,b762,c752]=trans_sl_from_vals_762(a778,a762,a7
52);

range=range_from_trans_762(transm,temperature,dew_pt,pressu
re);

    end;
```

This next section of code takes the information about the target signal locations and determines the average values for each frame. It then creates vectors of the signal for each band pass as well as retrieves the time stamp information. This also includes a low pass filter for removing large signal anomalies (over 10,000 counts above the average). Random high levels of noise were known to exhibit itself in the camera.

```
%%            Read Files and average the signal levels
function
[m2high,n2high,m2mid,n2mid,m2low,n2low,a2high,a2mid,a2low]=
read_labv22(year,month,day,folder,shigh,smid,slow,r1,r2)
temp=dir(strcat(folder,'/',shigh));
for i=1:(length(temp)-1)
data=imread(strcat(folder,'/',temp(i+1).name));
cdata=nuc_corr22(data);
mhigh(:,:,i)=cdata(r1,r2);
ahigh(i)=mean(mean(mhigh(:,:,i)));
timestr=strrep(temp(i+1).name,'-','.');
nhigh(i)=datenum(year,month,day,str2num(timestr(5:6)),str2n
um(timestr(7:8)),str2num(timestr(10:15)));
flaghigh(i)=median(cdata(:));
end
temp=dir(strcat(folder,'/',smid));
for i=1:length(temp)
data=imread(strcat(folder,'/',temp(i).name));
cdata=nuc_corr22(data);
mmiddle(:,:,i)=cdata(r1,r2);
amid(i)=mean(mean(mmiddle(:,:,i)));
timestr=strrep(temp(i).name,'-','.');
```

```
nmiddle(i)=datenum(year,month,day,str2num(timestr(5:6)),str
2num(timestr(7:8)),str2num(timestr(10:15)));
flagmid(i)=median(cdata(:));
end

temp=dir(strcat(folder,'/',slow));

for i=1:length(temp)
data=imread(strcat(folder,'/',temp(i).name));
cdata=nuc_corr22(data);
mlow(:,:,i)=cdata(r1,r2);
alow(i)=mean(mean(mlow(:,:,i)));
timestr=strrep(temp(i).name,'-','.');
nlow(i)=datenum(year,month,day,str2num(timestr(5:6)),str2nu
m(timestr(7:8)),str2num(timestr(10:15)));
flaglow(i)=median(cdata(:));
end

avhigh=median(flaghigh(:));
avmid=median(flagmid(:));
avlow=median(flaglow(:));

highcutoff=10000+avhigh;
midcutoff=10000+avmid;
lowcutoff=10000+avlow;

j=1;
for i=1:length(flaghigh);
    if flaghigh(i)<highcutoff;
         if flagmid(i)<midcutoff;
             if flaglow(i)<lowcutoff;
        m2high(:,:,j)=mhigh(:,:,i);
        a2high(j)=ahigh(i);
        n2high(j)=nhigh(i);

         m2mid(:,:,j)=mmiddle(:,:,i);
        a2mid(j)=amid(i);
        n2mid(j)=nmiddle(i);

        m2low(:,:,j)=mlow(:,:,i);
        a2low(j)=alow(i);
        n2low(j)=nlow(i);

        j=j+1;
             end
         end
    end;
end;
```

This next section of code takes the average signal intensities from each band pass and normalizes them for the filter line shape as well as the camera spectral response.

This also linearly interpolates the outer band passes, to get a baseline. Finally, the transmission is calculated from the ratio of the 762 nm band pass data to the baseline.

```
function
[trans,cor762,base762,cor752]=trans_sl_from_vals_762(m778,m
762,m752);

load constants/Norm_factors.mat;

cor778=m778;
cor762=m762.*c762./norm762.*norm778;
cor752=m752.*c752./norm752.*norm778;

base762=(cor778-cor752).*(10/26)+cor752;

trans=real(cor762./base762);
```

This final section of code takes the transmission value with the atmospheric conditions to lookup the range. This code first corrects the predefined path length vector model for the atmospheric conditions, and then compares the input transmission value to this corrected path length versus transmission fraction curve to estimate the target range.

```
function range=range_from_trans_762(trans,temp,dp,press);
%trans - %transmission temp and dew point in celcius and
pressure in
%millibar

load 'constants/transmission_data_new.mat';

tau=373.16/(dp+273.16);
vp=10^(-7.90298*(tau-1)+5.02808*log10(tau)-1.3816*(10^-
7)*(10^(11.344*(1-1/tau))-1)+8.1328*10^-3*(10^(-
3.4915*(tau-1))-1)+5.00571);
q=0.622*vp/(100*press-0.378*vp);
tv=(1+0.61*q)*(temp+273.16);
length=path_length.*(1./(press*.000986923267)).*(tv./300);
fit=spline(t762,length);
fit2=spline(length,t752);
fit3=spline(length,t778);
range1=ppval(fit,trans);
base752=ppval(fit2,range1);
base778=ppval(fit3,range1);
base762=(base778-base752)*10/26+base752;
range=ppval(fit,trans.*base762);
```

Bibliography

Anderson, Joel, Louis Szczukowski, Brandon Abel, Kip Johnson, and Ever Zavala. "Monocular Passive Ranging (Project Air Cyclops)", Technical Information Memorandum 09-10, Air Force Flight Test Center, Edwards AFB CA, December 2009.

Andrews, Larry, and Ronald Phillips. *Laser Beam Propagation through Random Media*. Bellingham Washington: SPIE – The International Society for Optical Engineering, 2005.

Evans, Howard E. and Brian A. Hibbeln. "The Theory of Single Sensor Altitude Determination," *Proceedings of the IEEE Aerospace Applications Conference*. 53-65. IEEE Press, March 1996.

Hasson, Victor H. and Christopher R. Dupuis. "Passive ranging through the Earth's Atmosphere," *Proceedings of the SPIE,* Vol 4538, 49-56. SPIE, 2002.

Hawks, Michael R. Passive ranging using atmospheric oxygen absorption spectra. Air Force Institute of Technology (AU), March 2006.

Jeffrey, William, James Draper, and Richard Gobel. "Monocular Passive Ranging," *Proceedings of IRIS Targets, Backgrounds, and Discrimination,* Vol II, 113-130. February 1994.

Rothman, Laurence, S. and others. "The HITRAN 2008 molecular spectroscopic database," *Journal of Quantitative Spectroscopy & Radiative Transfer*, 110:533-572 (June-July 2009).

Scriven, Gordon, and Nahum Gat. *Advanced Monocular Passive Ranging (AMPR) for HALO II: SBIR Phase II Final Report*, 29 December2003 - 28 December 2007. Contract FA9300-04-C0021. Torrance CA: Opto-Knowledge Systems, Inc., March, 2008.

Sprangle, Phillip, Joseph Peñano, and Bahman Hafizi. "Propagation of High Energy Laser Beams in Various Environments." NRL/MR/6790—07-9032. Naval Research Laboratory, Washington D.C., June 2007.

REPORT DOCUMENTATION PAGE

Form Approved
OMB No. 074-0188

1. REPORT DATE *(DD-MM-YYYY)*	**2. REPORT TYPE**	**3. DATES COVERED** *(From – To)*
25-03-2010	Master's Thesis	May 2007-March 2010

4. TITLE AND SUBTITLE

Monocular Passive Ranging by an Optical System with Band Pass Filtering

5a. CONTRACT NUMBER

5b. GRANT NUMBER

5c. PROGRAM ELEMENT NUMBER

6. AUTHOR(S)

Anderson, Joel R., Captain, USAF

5d. PROJECT NUMBER

5e. TASK NUMBER

5f. WORK UNIT NUMBER

7. PERFORMING ORGANIZATION NAMES(S) AND ADDRESS(S)
Air Force Institute of Technology
Graduate School of Engineering and Management (AFIT/EN)
2950 Hobson Way, Building 640
WPAFB OH 45433-8865

8. PERFORMING ORGANIZATION REPORT NUMBER

AFIT/GAP/ENP/10-M01

9. SPONSORING/MONITORING AGENCY NAME(S) AND ADDRESS(ES)
National Air and Space Intelligence Agency
John Florio
4180 Watson Way
Wright Patterson AFB, OH 45433-5648

10. SPONSOR/MONITOR'S ACRONYM(S)
NASIC/DAPM

11. SPONSOR/MONITOR'S REPORT NUMBER(S)

12. DISTRIBUTION/AVAILABILITY STATEMENT

APPROVED FOR PUBLIC RELEASE; DISTRIBUTION UNLIMITED.

13. SUPPLEMENTARY NOTES

14. ABSTRACT

An instrument for monocular passive ranging based on atmospheric oxygen absorption near 762 nm has been designed, built and deployed to track emissive targets, including the plumes from jet engines or rockets. An intensified CCD array is coupled to variable band pass liquid crystal display filter and 3.5 – 8.8 degree field of view optics to observe the target. By recording sequential images at 7 Hz in three 6 nm width bands, the transmittance of the R-branch of the O_2 (X-b) (0,0) band is determined. A metric curve for determining range from transmittance is developed using the HITRAN spectral database. A low cost system was designed and ground tested at ranges of 50 -380 m using halogen and incandescent light sources, establishing an average range error of 12%. The system was first deployed for a ground test viewing an F-16 in afterburner at ranges of 0.35 – 4.8 km, establishing a range error of 15% despite the presence of optical turbulence and a structured source spectrum. Finally, the instrument was flight tested in a C-12 imaging an F-16 in afterburner at ranges up to 11 km. The target was manually tracked, and pointing jitter limited image interpretation. A study of range error as a function of signal-to-noise ratio produced superior results to previous methods using Fourier Transform Spectroscopy. However, increased signal relative to background scatter will be required for accurate ranging for these tactical air-to-air scenarios. The promise for improved instrument performance is discussed.

15. SUBJECT TERMS

Monocular Passive Ranging	Flight Test	Ground Test
Oxygen Absorption	Airborne imaging	Near Infrared (NIR)
AFIT	TPS	

a. REPORT	**b. ABSTRACT**	**c. THIS PAGE**	**17. LIMITATION OF ABSTRACT**	**18. NUMBER OF PAGES**	**19a. NAME OF RESPONSIBLE PERSON**
					Dr. Glen Perram
U	**U**	**U**	**UU**	70	**19b. TELEPHONE NUMBER** *(Include area code)* (937) 255-6565, ext 4504 (glen.perram@afit.edu)

Standard Form 298 (Rev. 8-98)
Prescribed by ANSI Std. Z39-18